DAHLGREN DIVISION
NAVAL SURFACE WARFARE CENTER

Dahlgren, Virginia 22448-5100

NSWCDD/TR-98/113

AN EVALUATION OF PRECISE ABSOLUTE NAVIGATION (PAN) PERFORMANCE UNDER DYNAMIC CONDITIONS

BY BRUCE R. HERMANN

THEATER WARFARE SYSTEMS DEPARTMENT

JANUARY 1999

19990507 019

DTIC QUALITY INSPECTED 4

DTIC QUALITY INSPECTED 4

REPORT DOCUMENTATION PAGE

Public reporting burden for this collection of information is estimated to average 1 hour per response, including the time for reviewing instructions, search existing data sources, gathering and maintaining the data needed, and completing and reviewing the collection of information. Send comments regarding this burden or any other aspect of this collection of information, including suggestions for reducing this burden, to Washington Headquarters Services. Directorate for information Operations and Reports, 1215 Jefferson Davis Highway, Suite 1204, Arlington, VA 22202-4302, and to the Office of Management and Budget, Paperwork Reduction Project (0704-0188), Washington, DC 20503.

1. AGENCY USE ONLY (Leave blank)	2. REPORT DATE	3. REPORT TYPE AND DATES COVERED
	January 1999	Final

4. TITLE AND SUBTITLE

An Evaluation of Precise Absolute Navigation (PAN) Performance Under Dynamic Conditions

5. FUNDING NUMBERS

6. AUTHOR(s)

Bruce R. Hermann

7. PERFORMING ORGANIZATION NAME(S) AND ADDRESS(ES)

Commander
Naval Surface Warfare Center
Dahlgren Division (Code'T12)
17320 Dahlgren Road
Dahlgren, VA 22448-5100

8. PERFORMING ORGANIZATION REPORT NUMBER

NSWCDD/TR-98/113

9. SPONSORING/MONITORING AGENCY NAME(S) AND ADDRESS(ES)

10. SPONSORING/MONITORING AGENCY REPORT NUMBER

11. SUPPLEMENTARY NOTES

12a. DISTRIBUTION/AVAILABILITY STATEMENT

Approved for public release; distribution is unlimited.

12b. DISTRIBUTION CODE

13. ABSTRACT (Maximum 200 words)

This report describes a method where the Global Positioning System (GPS) Precise Positioning Service (PPS) solutions recorded in the field can be reprocessed at a later time with the precise ephemerides, without requiring that the observations be saved. The reprocessing with the precise ephemerides improves the quality of the navigation solutions compared with the solutions obtained when the real-time broadcast ephemerides are used.

This report continues the investigation of the Precise Absolute Navigation (PAN) technique by exploring its accuracy under two particular conditions. The first condition is operation with single-frequency observations and use of the broadcast ionospheric model; the second is when the user experiences appreciable height variations due to his motion, as in an aircraft. Also demonstrated are the accuracy of PAN solutions to simulated observations from a high-altitude, low-speed platform, such as an Unmanned Aerial Vehicle (UAV).

14. SUBJECT TERMS		15. NUMBER OF PAGES
Global Positioning System (GPS) Precise Absolute Navigation (PAN)	Precise Positioning Service (PPS) Unmanned Air Vehicle (UAV)	41
		16. PRICE CODE

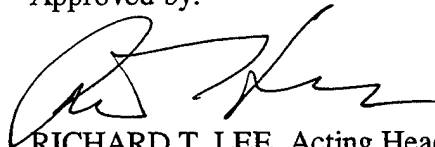| 17. SECURITY CLASSIFICATION OF REPORTS	18. SECURITY CLASSIFICATION OF THIS PAGE	19. SECURITY CLASSIFICATION OF ABSTRACT	20. LIMITATION OF ABSTRACT
UNCLASSIFIED	UNCLASSIFIED	UNCLASSIFIED	SAR

NSN 7540-01-280-5500

FOREWORD

A mission of the National Imagery and Mapping Agency (NIMA) requires that geodetic quality absolute positions be determined autonomously and in areas far removed from other sites. The use of Differential Global Positioning System (DGPS) techniques or relative positioning is sometimes precluded. Keyed Global Positioning System (GPS) receivers can output Precise Positioning Service (PPS) navigation solutions. Because they are computed in real time, PPS solutions necessarily use the broadcast ephemerides and, consequently, are subject to ephemeris and satellite-clock prediction errors. The PPS solutions can be recorded, but the broadcast ephemerides and the observations, when corrected for Selective Availability (SA), cannot. This report demonstrates, through simulations, that field-recorded PPS solutions can be reprocessed with the more accurate precise ephemerides. Reprocessing with the precise ephemerides offers improved navigation solutions, but does not require that the SA-corrected pseudorange or phase observations be saved. The method is called Precise Absolute Navigation (PAN). This report continues the evaluation of the PAN algorithm which has been described in previous documentation.

Support for this development was provided by NIMA under the direction of Mr. Kenneth Croisant and Mr. Stephen Malys.

The author wishes to thank Dr. Randall Smith of NIMA for suggesting this technique as one of interest to NIMA for particular applications. The author also wishes to thank the following individuals at the NIMA Center in St. Louis for assisting in the development of PAN: Mr. Angus Jones, Mr. Brian Tallman, and Mr. Brian Deem, for providing data and suggestions; and Ms. Lisa McCormick for processing data sets through the Data Correction Facility (DCF). Special assistance from Captain Gottschalk and Mr. C. H. Cook at the Master Control Station was also invaluable.

This final report for FY97 has been reviewed by Mr. Everett Swift, Program Manager for NIMA related projects; Dr. Jeffery Blanton, Head, Space Systems Applications Branch; and Mr. James Sloop, Head, Space and Weapons Systems Analysis Division.

Approved by:

RICHARD T. LEE, Acting Head
Theater Warfare Systems Department

CONTENTS

ILLUSTRATIONS

TABLES

1.0 INTRODUCTION

The purpose of the Precise Absolute Navigation (PAN) development is to investigate the feasibility of improving, by postprocessing, the accuracy of a set of typical Precise Positioning Service (PPS) navigation solutions from keyed receivers. Real-time, stand-alone navigation solutions necessarily use the broadcast ephemerides as the source of the satellite position and satellite clock estimates. However, in certain cases, the particular mission could benefit from more accurate navigation solutions. If the mission is not time critical, it may be acceptable to delay the improvement of the navigation solutions until the postfit precise ephemerides are available. In this case, significantly better results can be expected.

With precise ephemerides, static absolute position solutions can achieve submeter repeatability [1], [2]. Meter-level navigation solutions have been demonstrated by postprocessing L_1 observations with postfit precise ephemerides, clock estimates, and an ionospheric model [3]. Applications where PANs would be of interest include cases where auxiliary data for differential or relative solutions are not available, or where the track of a moving vehicle or ship is desired at remote locations far from other sites.

In the operational environment, the PPS navigation solutions will be obtained from a keyed receiver. A keyed receiver will be able to correct for the effects of Selective Availability (SA) and AntiSpoofing (AS) that are intentionally introduced into the system. AS encrypts and SA corrupts the Global Positioning System (GPS) signals, making the precise signal and the full accuracy of the broadcast ephemerides accessible to authorized users only. These receivers can display the navigation solution in real time, but the field-corrected satellite ephemerides, and the SA-corrected pseudorange and phase observations are classified and, therefore, are not available to the user. The PPS position solutions are unclassified and can be recorded in the field, along with the GPS time and the satellites contributing to the solution. Even though the original observations are lost, this information is enough to allow the PPS solutions to be improved at a later time with the postfit precise ephemerides.

Section 2 outlines the mathematical method used to produce the PAN solutions. The accuracy of PAN is evaluated in Section 3 by investigating two particular performance questions. Finally, in Section 4, a simulation of high-altitude solutions, as from an Unmanned Aerial Vehicle (UAV), were performed. The results from these tests are presented.

2.0 METHOD

For this description of the method, it will be assumed that the GPS time and the PPS solutions to be improved are given, as is the receiver type and the details of the navigation algorithm it used. The algorithm information may be needed to establish which satellites, of those in view, produced the particular navigation solution. Alternately, the field receiver may be able to supply the satellite PRN

numbers that were tracked. To compute the difference between the two ephemerides, an independent source of the SA-corrected broadcast ephemerides, and the NIMA precise ephemerides and clock estimates are required. Finally, for testing purposes, two-frequency SA-corrected pseudorange and phase observations from a typical receiver need to be added to the requirements listed above.

2.1 SPS Solutions

The form of the observation equations that produces the Standard Positioning Service (SPS) navigation solution in the field receiver can be reconstructed as in Equation (1). The original observation vector at time t_k is denoted by O_k. The ranges computed from the satellite ephemerides and the estimate of the current state $\tilde{X}_k$ are placed in the C_{bk} vector. The inherently nonlinear problem is then linearized by writing the observation vector equal to the first two terms of the Taylor series expansion for C_{bk}.

$$O_k = C_{bk} + \frac{\partial C_{bk}}{\partial X_k} \Delta X_{bk} + \epsilon_{bk} \tag{1}$$

The last term, ϵ_{bk}, represents the contributions from the terms that are ignored, plus the noise on the observations. The solution to Equation (1) is ΔX_{bk}, which is found by least squares in the usual way, as indicated in Equation (2). The W is the observation weight matrix that may be incorporated into the formulation.

$$\Delta X_{bk} = (A^T W A)^{-1} A^T W (O_k - C_{bk}) \tag{2}$$

The matrix A in Equation (2) represents the matrix of partials written as $\dfrac{\partial C_{bk}}{\partial X_k}$ in Equation (1).

From this result, the SPS state estimate $\hat{X}_{bk}^{SPS}$ can be found by adding the state update to the current state estimate: $\hat{X}_{bk}^{SPS} = \tilde{X}_k + \Delta X_{bk}$. It is worth noting that if the precise ephemerides were available in the field along with the broadcast ephemerides, the observation vector O_k could have been used with either of these ephemerides to produce an SPS position solution. This property will be invoked in Section 2.3 to derive the PAN algorithm.

2.2 PPS Solutions

The PPS user forms and solves the same sort of equations as the SPS user. The difference is that corrections for SA effects are included. AS will not be discussed since it has no direct effect on the PAN algorithm. AS may deny certain classes of receivers access to two-frequency observations and the ionospheric correction. It also denies the use of the precision available from P-code observations. The PPS user's receiver is assumed to be able to recover the two-frequency P-code and use it in the observation vector.

The PPS receiver applies the dither corrections to the pseudorange and phase observations. When applied, the original observation vector O_k is changed to $\acute{O}_k$. The receiver also applies the epsilon corrections to the broadcast ephemeris messages. The corrections appear in the satellite position part of the C_{bk} vector and changes it to the $\acute{C}_{bk}$ vector. Note that both of these SA-corrected vectors are required for a field PPS solution, but neither can be saved for later use. From thereon, the route to the PPS solutions proceeds in the same fashion as for the SPS. The PPS observation equation is the same as Equation (1) except that the corrected vectors are used. This is shown in Equation (3).

$$\acute{O}_k = \acute{C}_{bk} + \frac{\partial \acute{C}_{bk}}{\partial X_k} \Delta \acute{X}_{bk} + \acute{\epsilon}_{bk} \tag{3}$$

When this equation is solved by least squares in the same manner as before, the PPS state vector $\hat{X}_{bk}^{PPS}$ is found from the sum: $\hat{X}_{bk}^{PPS} = \tilde{X}_k + \Delta \acute{X}_{bk}$.

2.3 PPS With Precise Ephemerides

Suppose that precise ephemerides were available in the field when the PPS solution was computed. Its observation equation would be as shown in Equation (4), where the subscript p on C_{pk} denotes that the satellite positions originate from the precise ephemerides. There is no need for an epsilon correction to the postfit precise ephemerides, but the observation vector, on the left, is the same as the dither-corrected vector used in Equation (3).

$$\acute{O}_k = C_{pk} + \frac{\partial C_{pk}}{\partial X_k} \Delta X_{pk} + \epsilon_{pk} \tag{4}$$

Since this observation vector is common to Equations (3) and (4), they can be equated. This is shown in Equation (5).

$$\acute{\epsilon}_{bk} + \acute{C}_{bk} + \frac{\partial \acute{C}_{bk}}{\partial X_k} \Delta \acute{X}_{bk} = C_{pk} + \frac{\partial C_{pk}}{\partial X_k} \Delta X_{pk} + \epsilon_{pk} \tag{5}$$

From Equation (3) the PPS field solution $\hat{X}_{bk}^{PPS}$ is known. Therefore, it can be used in Equation (5) in place of the initial estimate $\tilde{X}_k$. New computed vectors are needed to reflect the change in the initial state estimate, these are indicated by the PPS superscript. This substitution does not change the equality as long as the observation vector remains unchanged, and the linearity

constraint continues to be satisfied. The new form for Equation (5), incorporating the PPS position, is shown in Equation (6).

$$\acute{C}_{bk}{}^{PPS} + \frac{\partial \acute{C}_{bk}{}^{PPS}}{\partial X_k} \Delta \acute{X}_{bk} = C_{pk}{}^{PPS} + \frac{\partial C_{pk}{}^{PPS}}{\partial X_k} \Delta X_{pk} + \epsilon_{pk}{}^{PPS} \tag{6}$$

If $\hat{X}_{bk}^{PPS}$ were used in Equation (3) instead of $\tilde{X}_k$, and the system were solved, the new state solution would be near zero. This result is usually called the adjusted Observed minus Computed residual and reflects the level of observation noise and other unmodeled effects. Therefore, the second term from the left in Equation (6) can be neglected because the state vector $\Delta \acute{X}_{bk}$ is approximately zero. When this is the case, Equation (6) reduces to a simpler form shown in Equation (7).

$$\acute{C}_{bk}{}^{PPS} \approx C_{pk}{}^{PPS} + \frac{\partial C_{pk}{}^{PPS}}{\partial X_k} \Delta X_{pk} + \epsilon_{pk}{}^{PPS} \tag{7}$$

This equation can be solved by least squares for ΔX_{pk} in an expression like Equation (2). Equation (8) shows the result with the weight matrix replaced by the identity I, implying that the PPS solutions from each epoch are equally weighted.

$$\Delta X_{pk} = (A^T I A)^{-1} A^T I (\acute{C}_{bk}{}^{PPS} - C_{pk}{}^{PPS}) \tag{8}$$

Then the improved state, with the quality of the postfit precise ephemerides, is $\hat{X}_{pk}$ and is found from the sum: $\hat{X}_{pk} = \hat{X}_{bk}{}^{PPS} + \Delta X_{pk}$. This is the PAN solution. The foregoing argument is equivalent to noting in Equation (3) that when $\Delta \acute{X}_{bk}$ is zero, the vector $\acute{C}_{bk}$ plus some noise $\acute{\epsilon}_{bk}$ is equal to the observation vector. Therefore, it is possible to approximately recreate the lost observations from knowledge of the satellite ephemerides and the solution vector $\hat{X}_{bk}^{PPS}$ [4].

3.0 PAN EVALUATION

PAN assumes that PPS field solutions exist, so the first task on the way to verification of the method was to generate simulated PPS solutions from GPS observations already on hand. This required that a navigation algorithm be developed and tested. The solutions obtained from the navigation algorithm were intended to substitute for the PPS field solutions that are the starting point

for the PAN algorithm. The navigation solutions require GPS observations. Two sources of existing observations and their results were described in a previous report [5].

This section of the report presents the answers to two particular questions concerning the performance of PAN. The first is the capability to obtain improved solutions using only single-frequency observations and the broadcast ionospheric model. The second is vertical accuracy when the user is experiencing considerable height variations.

3.1 Single-Frequency Operation

If PPS solutions are obtained only on L_1, the ionospheric effect is not compensated by the usual two-frequency correction. Instead, the broadcast message provides eight coefficients that are used in a model described by Klobuchar [6], [7]. Comparisons will be made between the computed two-frequency correction and the following cases:

1. Single-frequency L_1 only
2. Solutions using half the computed two-frequency correction
3. Solutions using 1.5 times the computed two-frequency correction
4. The Klobuchar model

The propagation delay introduced into the GPS signals by the ionosphere is a function of frequency, and its magnitude is correlated with solar activity. The fact that the delay is frequency dependent allows observations at two well-separated frequencies to remove the bulk of the effect. Thus the GPS was designed to transmit on L_1 (1575.42 MHz) and L_2 (1227.60 MHz) so that users desiring high-accuracy positions could use the two observations to remove the ionospheric delay.

To see how this is accomplished, the pseudorange observations ρ_i can simply be modeled as the sum of the ionospheric-free pseudorange r and the frequency-dependent ionospheric delay $\dfrac{K}{f_i^2}$, as is shown in Equation (9). The subscript i ($= 1$ or 2) indicates that the frequency is either L_1 or L_2, and K is a parameter proportional to electron density, which sets the magnitude of the delay.

$$\rho_i = r + \frac{K}{f_i^2} \tag{9}$$

If the two equations like Equation (9) are solved for K, the result is shown in Equation (10).

$$K = \frac{f_1^2 f_2^2}{f_2^2 - f_1^2} (\rho_1 - \rho_2) \tag{10}$$

5

Now, with K known, it can be substituted back into the original equation for L_1 or L_2 to compute the ionospheric-free pseudorange shown in Equation (11).

$$r = \frac{f_1^2}{f_1^2 - f_2^2} \rho_1 - \frac{f_2^2}{f_1^2 - f_2^2} \rho_2 \tag{11}$$

The ionospheric term is called the group delay and is proportional to the total electron content of the ionosphere N_T in TEC units of 10^{16} electrons/m², and f is in Hz. The group delay (in meters) is shown in Equation (12). It is clear that the K parameter used above is the same as $40.3 \times N_T$.

$$group\ delay = \frac{40.3\ N_T}{f^2} \tag{12}$$

The total electron content depends upon the solar radiation flux, which is related to the solar activity. A convenient measure of the solar activity is the sunspot number, which has been tracked for centuries. A plot of the raw sunspot counts since 1850 is shown in Figure 1. At the time of this writing, the solar sunspot number is emerging out of its minimum from the previous cycle and is beginning cycle 23. The two test data sets that will be used to evaluate the Klobuchar model are from dates near the minimum solar activity. These are plotted as vertical lines in Figure 2, which also illustrates the raw sunspot counts since 1980. Tests by others during periods of high solar activity have been generally favorable toward the accuracy of the model. In particular, S. P. Newby and R. B. Langley tested the Klobuchar model and the eight broadcast parameters, along with three other models during 1991 at several Canadian sites [8].
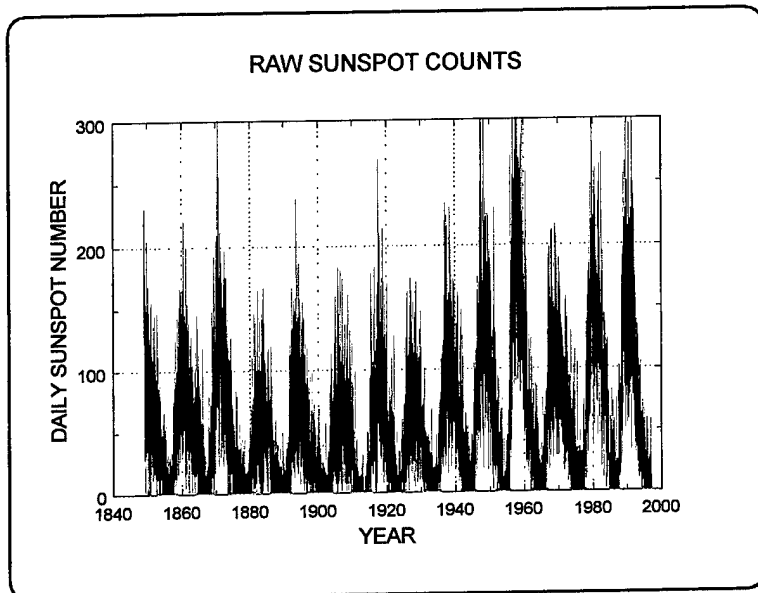

Figure 1— Sunspot Counts

An example of the total electron content computed from two-frequency observations at a static site is shown in Figure 3 for PRN16 on day 237 of 1995 at Site MSI (Corpus Christi, Texas). The elevation angle of the satellite is also plotted in the figure. The group delay in meters per TEC unit at each frequency is 0.162 and 0.267 m at L_1 and L_2, respectively. The fine structure in the TEC curve may in fact be partially due to multipath instead of actual TEC time and space variations. Whatever

the cause, the short-term variations cannot be realized by the model; instead, a smooth curve through the mean of the structure is the result from the model. The TEC for the next day 238 is shown in Figure 4. There is little change in the shape of the TEC between the two days. The two figures show that the model is approximately parallel to, but offset from, the two-frequency computation. Any constant offset between the model and reality is not as important as its relative performance satellite-to-satellite. Any constant offset that is common to all satellites will be treated as part of the local clock offset and does not produce a position error.
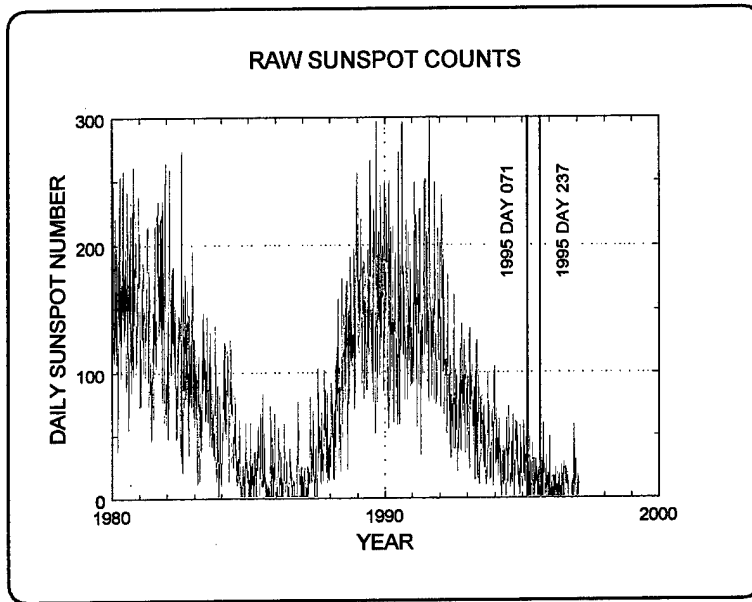

Figure 2— Times During Sunspot Cycle For Test Data Sets

As described in ICD-GPS-200, in order to use the Klobuchar model, the user needs to know the azimuth and elevation angles from the user to the satellite, the user's geodetic longitude and latitude, the current GPS time and the eight coefficients found in the broadcast message on page 18 of subframe 4.

3.2 Comparison of Results

To perform the comparison between the position solutions obtained from the Klobuchar broadcast model and from the two-frequency correction, data obtained from The Applied Research Laboratory at the University of Texas at Austin (ARL:UT) were used. These observations were obtained from a receiver at a static site on days 237 and 238 near Corpus Christi, Texas, in 1995. The observations are at 5-s epochs and include a 24,845-s span on day 237 and a 22,330-s span on day 238. The observations were sent to the NIMA Data Correction Facility (DCF) to
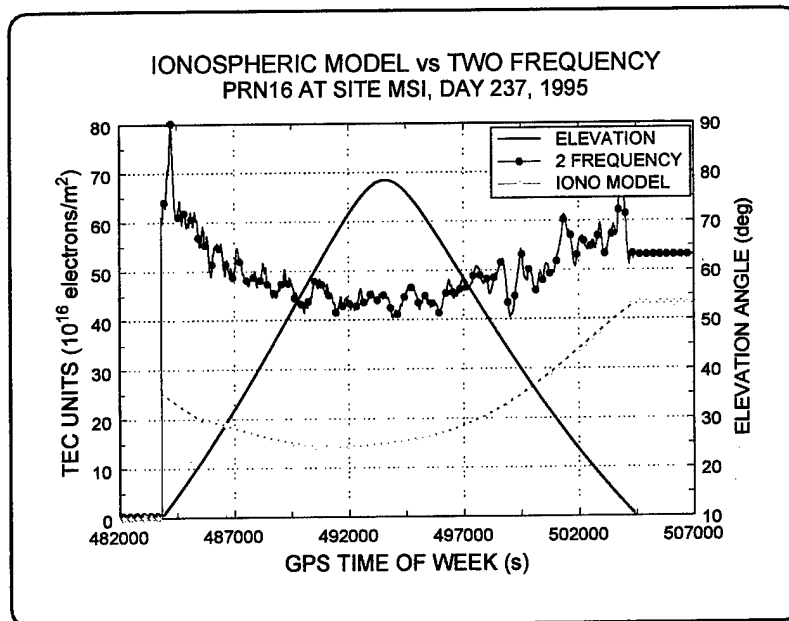

Figure 3— TEC For PRN 16 on Day 237

IONOSPHERIC MODEL vs TWO FREQUENCY
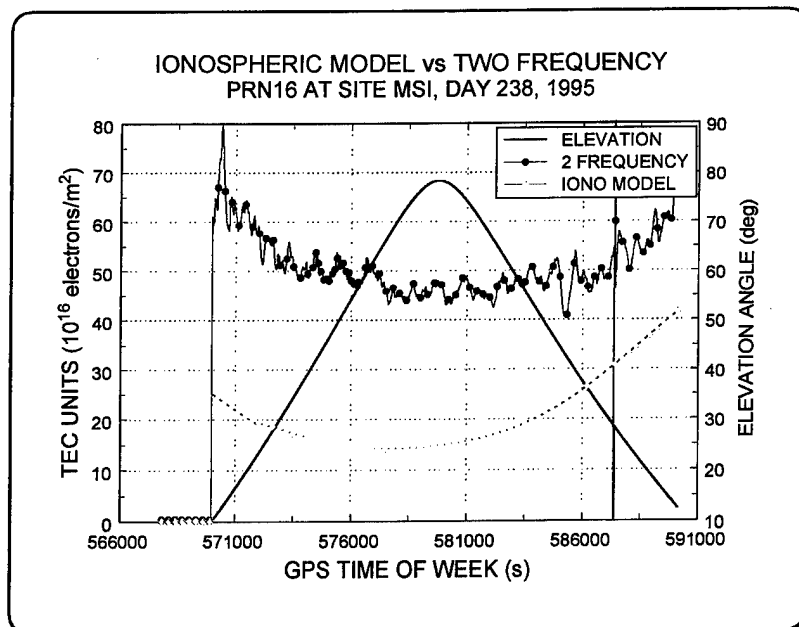PRN16 AT SITE MSI, DAY 238, 1995

Figure 4— TEC For PRN 16 on Day 238

be corrected for SA. These corrected observations were used to compute simulated PPS solutions for use by the PAN algorithm. Ionospheric model coefficients for that period were obtained through the NIMA representative at the Master Control Station located near Colorado Springs, Colorado.

Truth was obtained from the surveyed position of the site. Any systematic disagreement between the truth position and the PAN position is likely due to an error in the surveyed absolute coordinates of MSI. Solutions from simulated PPS and the PAN algorithm are presented for each of the three components: east, north, and vertical. In each figure, the five solutions are presented as crosshatched histograms overlaid on each other. The vertical axis indicates the fraction (in percent) of the total area under each bar. The sum over all bars equals 100%. Figures 5 through 7 show the weighted PPS solutions in each of the components for day 237. Figures 8 through 10 show the weighted PAN solutions for day 237. The PAN solutions were more tightly bunched than the PPS solutions. This reflects the more precise positioning achievable with the precise ephemerides. In the east component (Figure 8), all five peaks are within a meter. In the north component (Figure 9), there is a wider spread. The L_1-only peak tends to be the northernmost, with the other three being shifted farther south in order of the amount of the two-frequency correction applied. The result from the model shows two peaks straddling the peak in the full two-frequency correction. As is usually the case, the vertical solutions are more spread out than the others, but again there is a separation by the amount of the two-frequency correction applied. The L_1-only is the highest, with the other three being lower. The ionospheric model tends to agree with the full two-frequency correction in this case. The solutions are adjusted to give less weight to epochs where the geometic dilution of precision (GDOP) is greater than six.

Similar comments apply to day 238. Figures 11 through 13 show the PPS solutions in each component, and Figures 14 through 16 show the PAN solutions. The east component, Figure 11, shows a dual-peaked result, which disappears in Figure 14 with the precise ephemerides. The PPS north solutions, Figure 12, are widely spread but form a tighter bundle with the PAN solutions in Figure 15. The separation of the vertical solutions by the amount of ionospheric correction applied for day 238 is well illustrated in Figure 16. Generally, the solutions produced by the model and the two frequency correction agree well. A summary table for both days appears as Tables 1 and 2. The average values and the standard deviations are plotted for each component and each type of solution in Figures 17 and 18 for day 237, and Figures 19 and 20 for day 238. The averages show that the model is in better agreement with the full two-frequency correction than L_1-only, half the full two-frequency correction, or 1.5 times the full two-frequency correction.

8
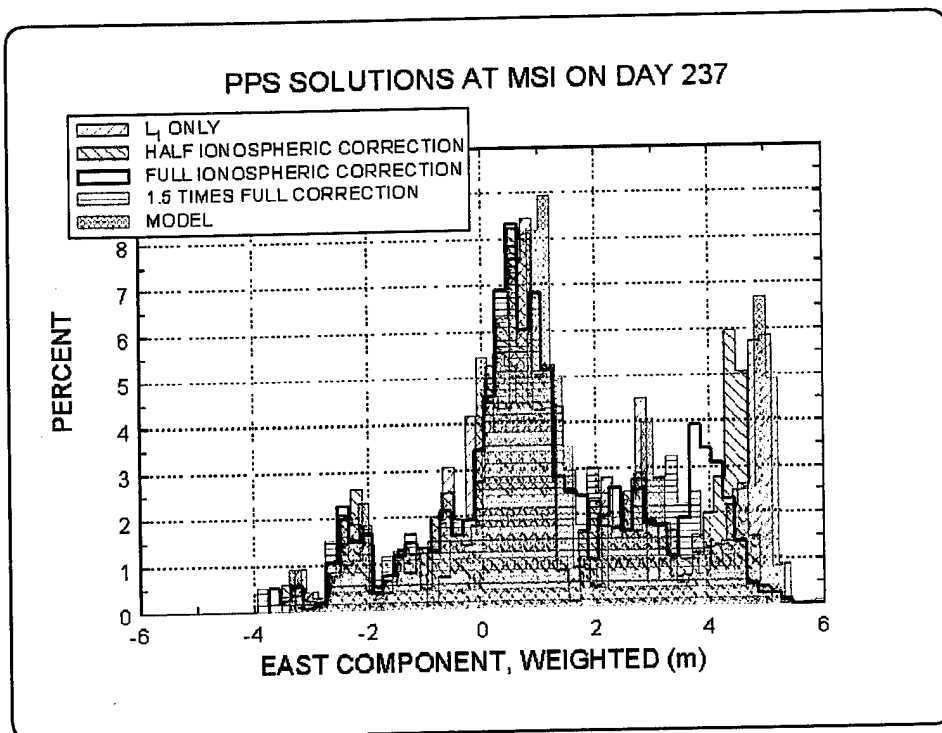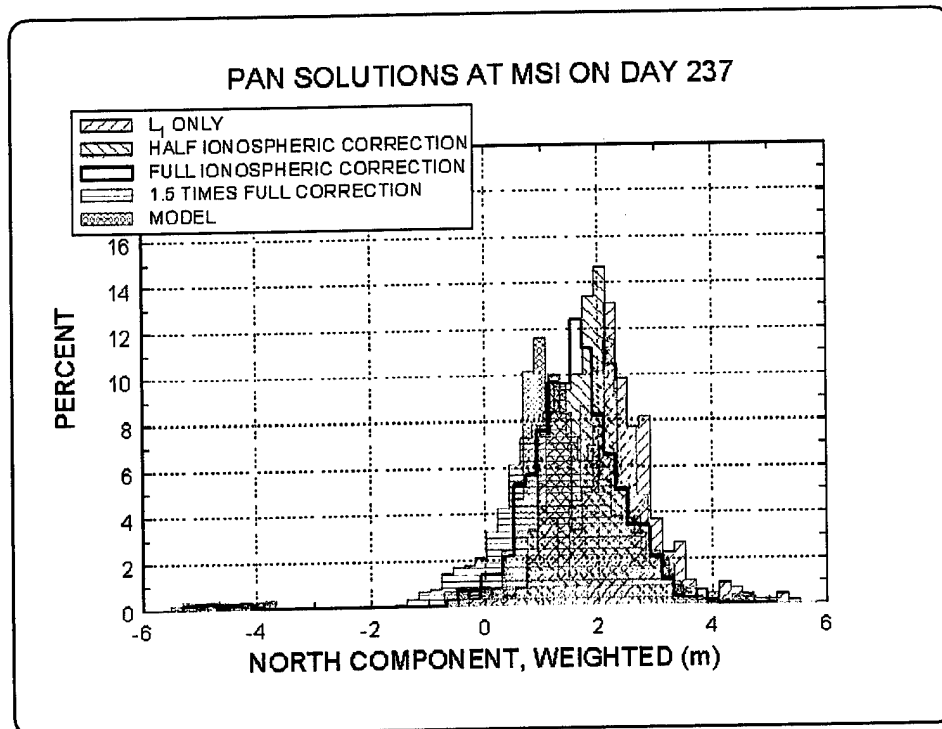
Figure 5— PPS East Component, Day 237
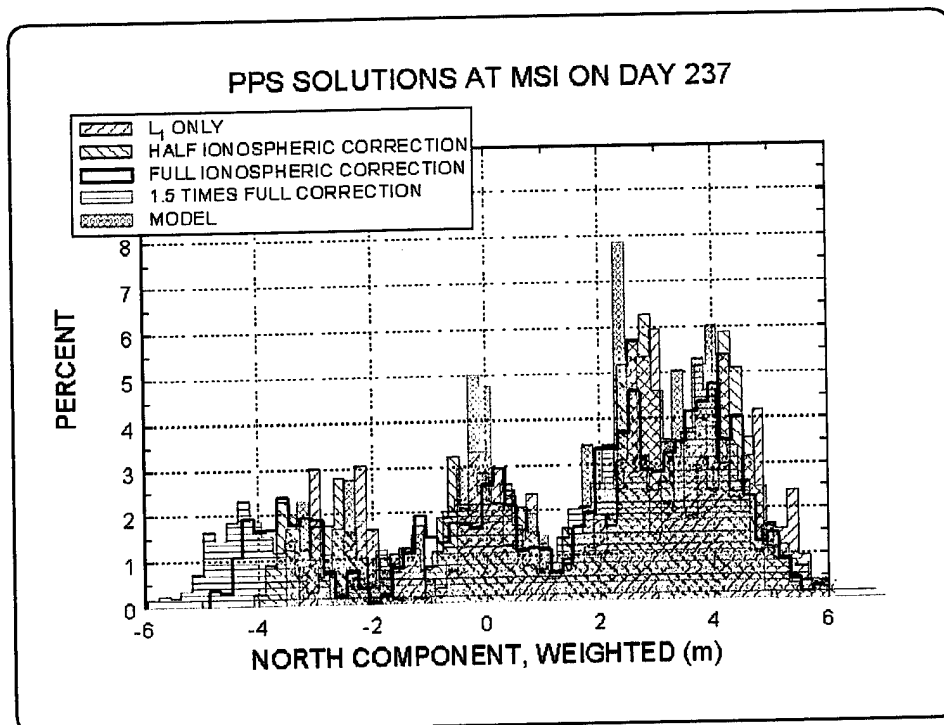
Figure 6— PPS North Component, Day 237

Figure 7— PPS Vertical Component, Day 237

Figure 8— PAN East Component, Day 237
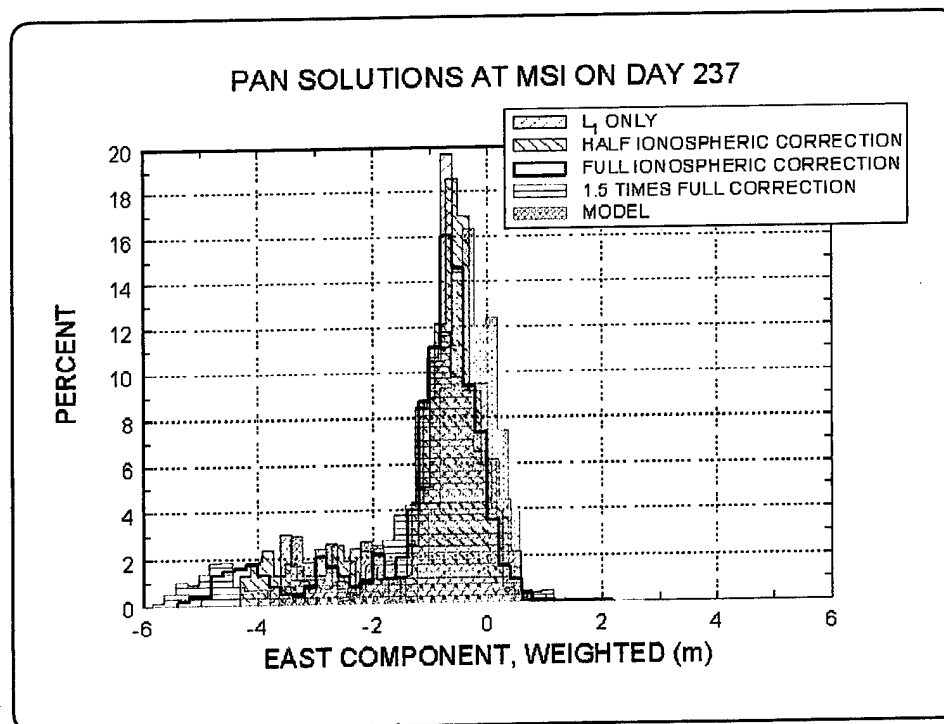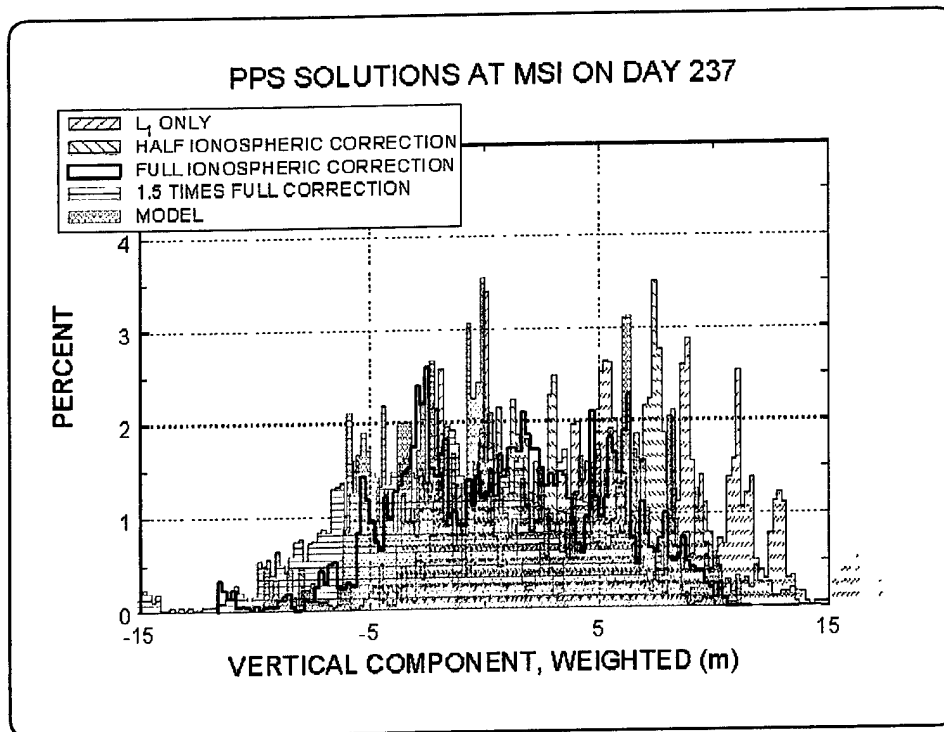
Figure 9— PAN North Component, Day 237
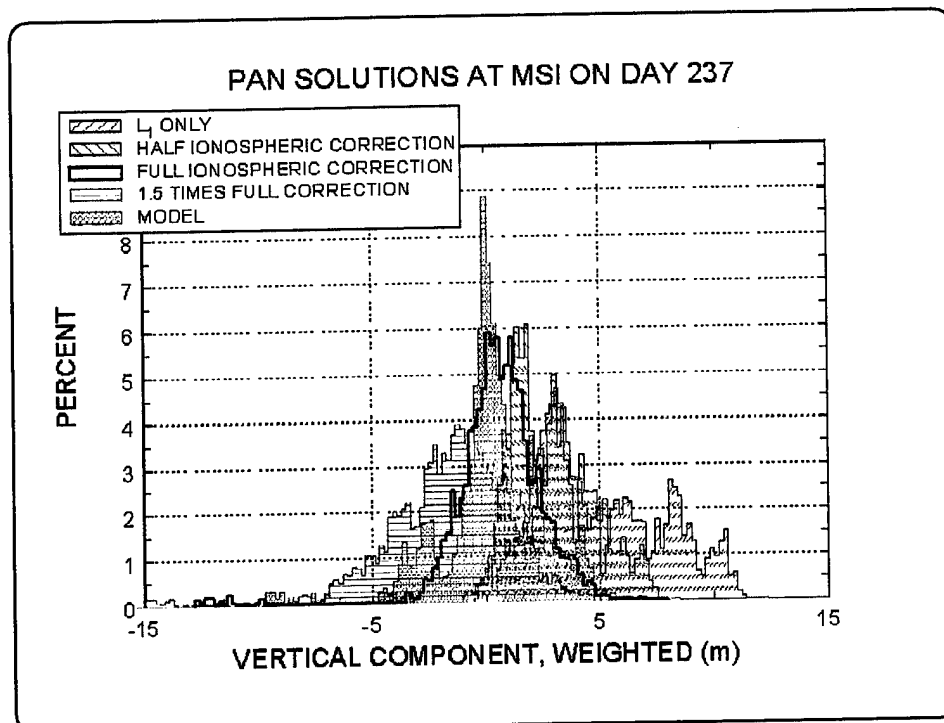
Figure 10— PAN Vertical Component, Day 237
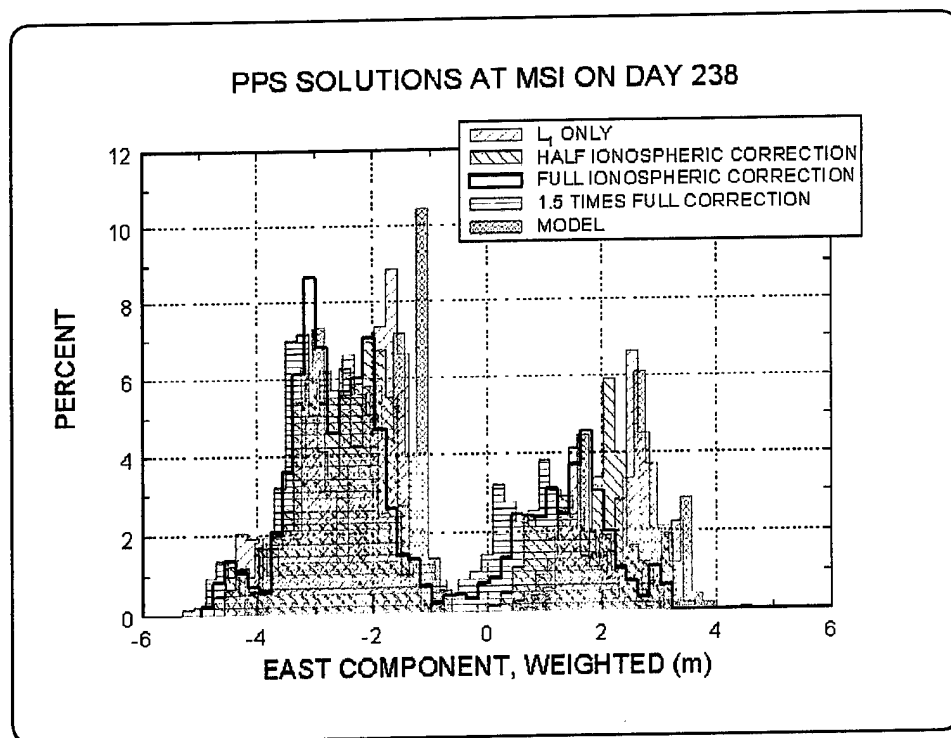
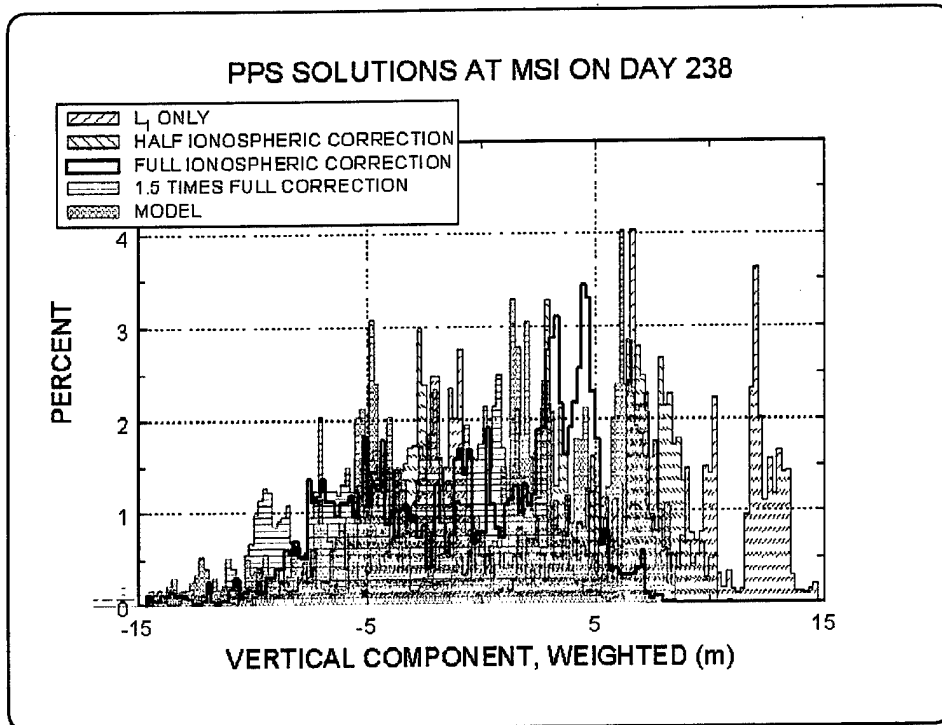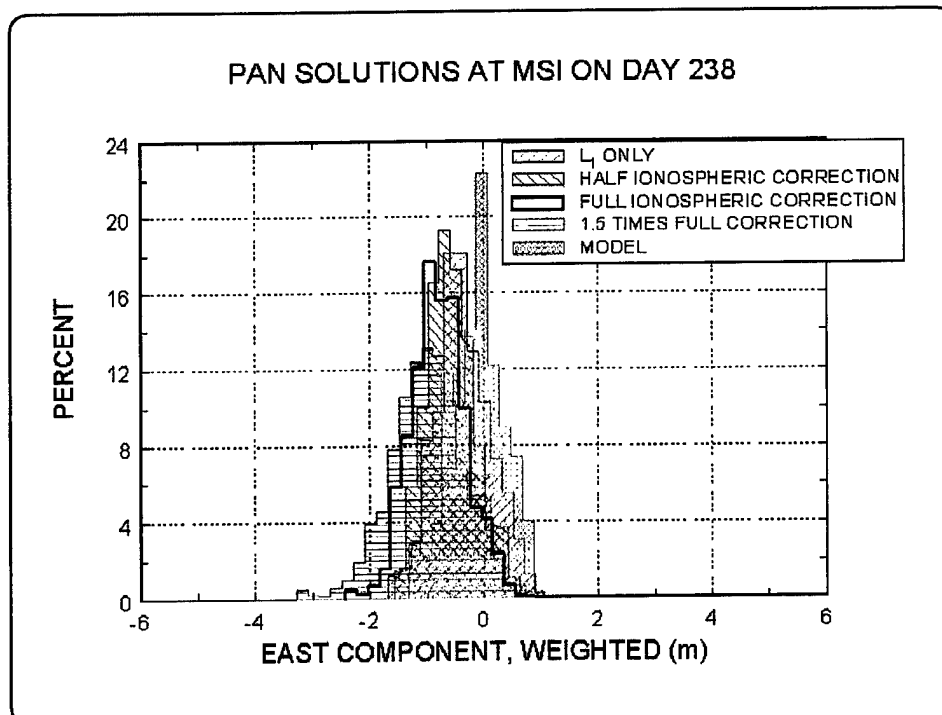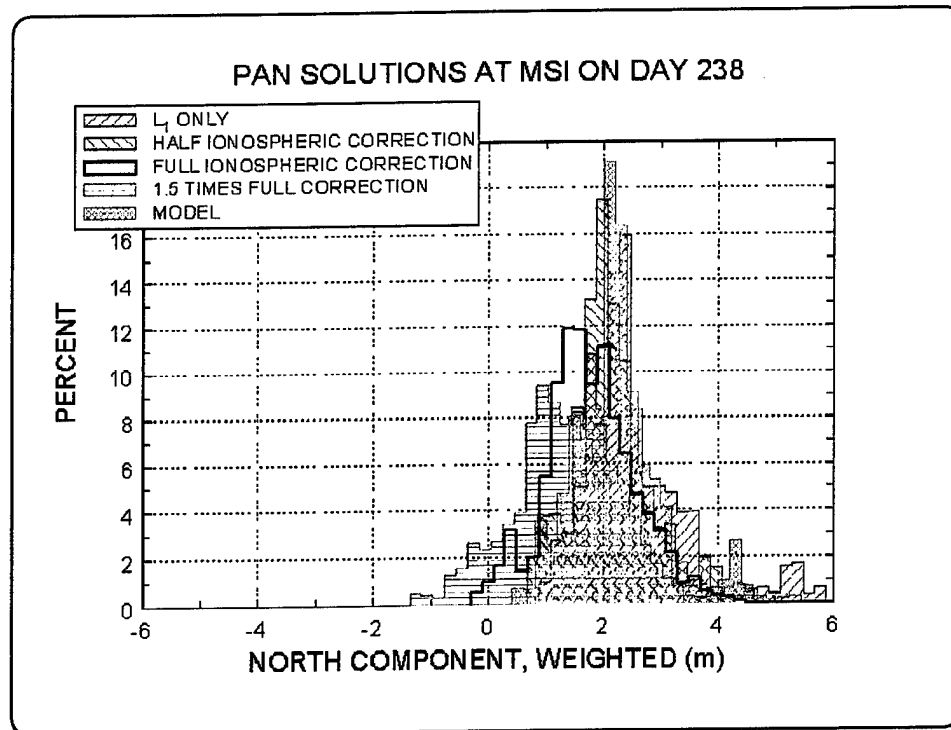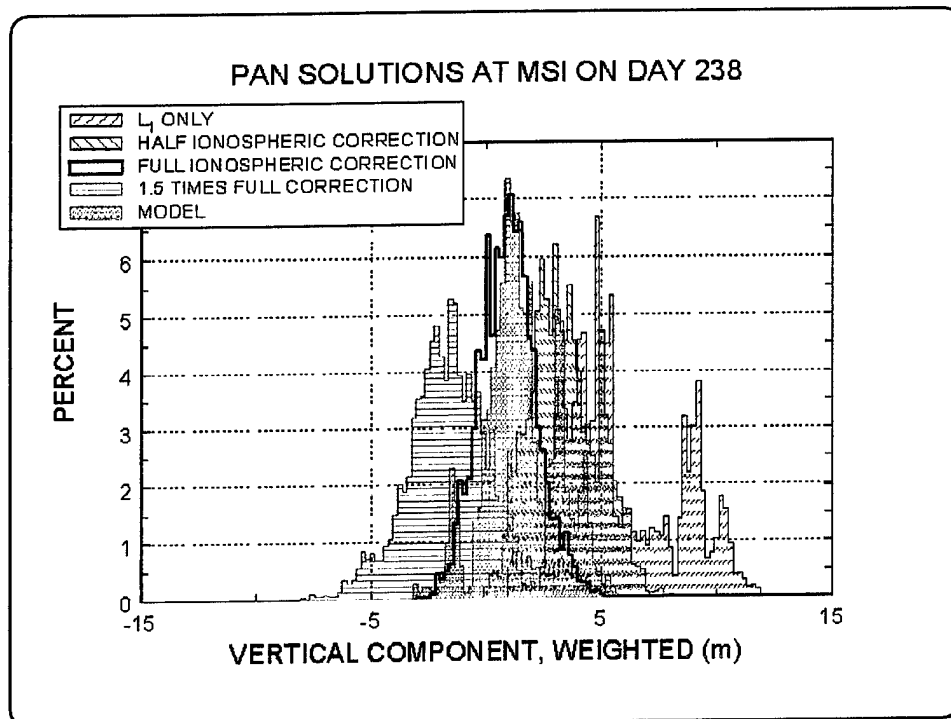**Figure 11—** PPS East Component, Day 238
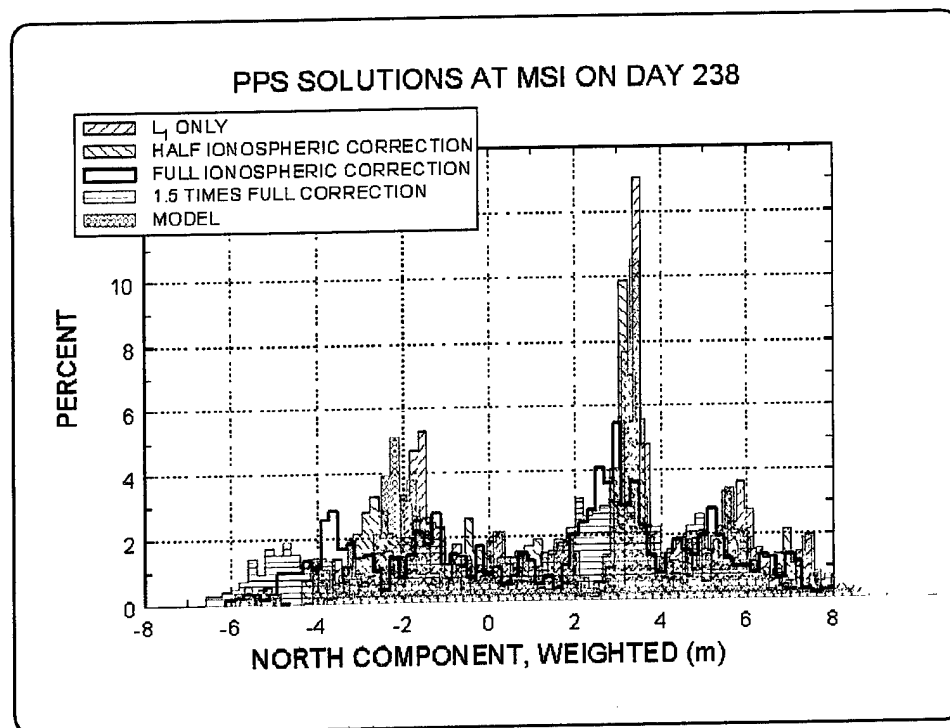
Figure 12— PPS North Component, Day 238

Figure 13— PPS Vertical Component, Day 238


Figure 14— PAN East Component, Day 238

PAN SOLUTIONS AT MSI ON DAY 238

Figure 15— PAN North Component, Day 238

PAN SOLUTIONS AT MSI ON DAY 238

Figure 16— PAN Vertical Component, Day 238

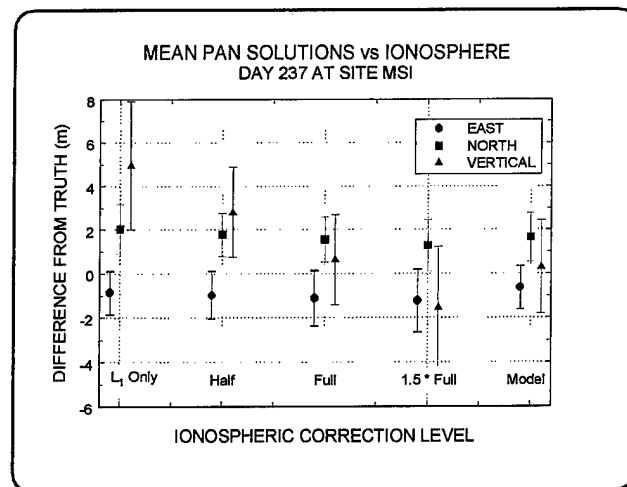**Table 1**—Means and Standard Deviations for Each Component on Day 237 at MSI

Units = meters	EAST				NORTH				VERTICAL			
	PPS		PAN		PPS		PAN		PPS		PAN	
	MEAN	S.D.	MEAN	S.D.	MEAN	S.D.	MEAN	S.D.	MEAN	S.D.	MEAN	S.D.
L_1 only	1.37	2.17	-0.90	0.98	1.89	2.46	2.00	1.13	5.25	4.88	4.89	2.96
Half Correction	1.25	2.02	-1.02	1.08	1.64	2.60	1.75	0.98	3.10	4.43	2.74	2.08
Full Correction	1.12	1.90	-1.16	1.25	1.39	2.80	1.53	1.04	0.94	4.41	0.58	2.05
1.5 × Correction	1.00	1.81	-1.26	1.42	1.14	3.04	1.25	1.17	-1.22	4.83	-1.58	2.72
Model	1.59	2.15	-0.68	0.98	1.52	2.28	1.63	1.11	0.60	4.77	0.24	2.12

Table 2—Means and Standard Deviations for Each Component on Day 238 at MSI

Units = meters	EAST				NORTH				VERTICAL			
	PPS		PAN		PPS		PAN		PPS		PAN	
	MEAN	S.D.	MEAN	S.D.	MEAN	S.D.	MEAN	S.D.	MEAN	S.D.	MEAN	S.D.
L_1 only	-0.91	2.35	-0.37	0.49	2.11	3.26	2.53	0.92	4.23	6.16	5.76	2.46
Half Correction	-1.11	2.20	-0.58	0.43	1.74	3.34	2.16	0.74	1.83	5.37	3.37	1.56
Full Correction	-1.32	2.07	-0.78	0.50	1.37	3.48	1.80	0.81	-0.57	4.79	0.97	1.45
1.5 × Correction	-1.52	1.96	-0.99	0.67	1.01	3.66	1.43	1.08	-2.96	4.51	-1.43	2.26
Model	-0.66	2.31	-0.12	0.47	1.78	3.35	2.21	0.75	-0.03	5.59	1.51	1.60
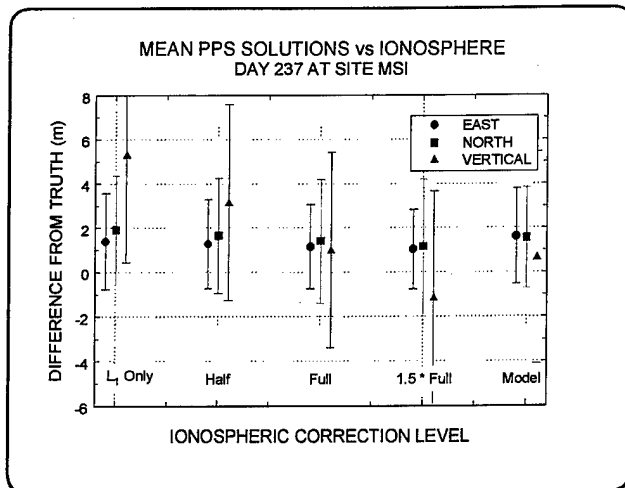
Figure 17— PPS Means and Standard
Deviations at MSI on Day 237

Figure 18— PAN Means and Standard
Deviations at MSI on Day 237
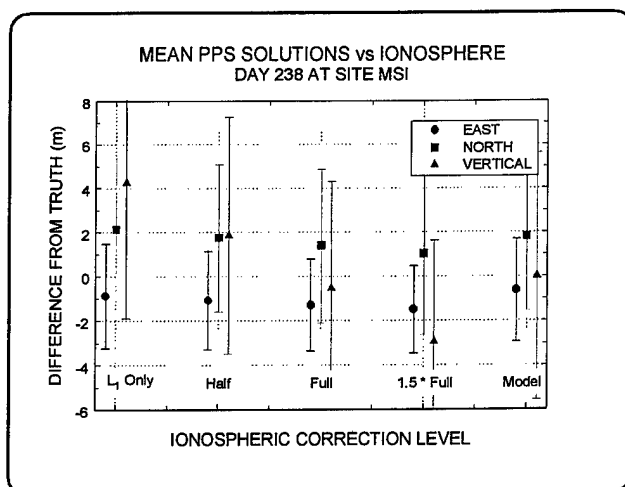
Figure 19— PPS Means and Standard
Deviations at MSI on Day 238

Figure 20— PAN Means and Standard
Deviations at MSI on Day 238

3.3 Ionospheric Model Summary

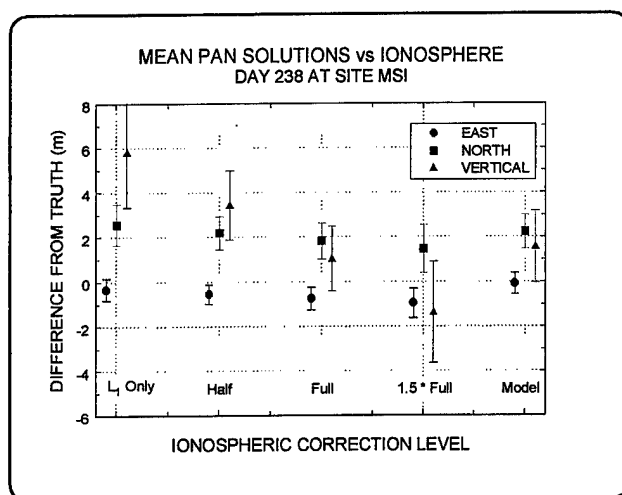At the current sunspot minimum, the east and north PAN solutions are not greatly affected by the value of the ionospheric correction; however, the vertical component is. The solutions appear to be too high when the ionospheric correction is neglected and too low when overcorrected. In general, the broadcast model results agree well with the two-frequency corrected solutions. Periods of high solar activity have not been tested here, but other investigators indicate that the model performs well under a variety of conditions.

The results of this study show that solutions based on single-frequency pseudoranges corrected by the broadcast ionospheric model can produce solutions with PAN that rival the two-frequency corrected solutions.

3.4 Pan Performance with Altitude Variations

Potential applications of PAN include those in which the ellipsoid height of the user is desired. Because height is the component that is most difficult to determine with GPS, it is of interest to test the PAN algorithm in the case where the user's height varies over a considerable range. The question to be answered is whether the user's vertical motion introduces additional errors that a static user does not experience.

Analysis of the solutions derived from the data obtained from ARL:UT is a good place to test the height performance. On days 237 and 238 of 1995, one static reference site and two aircraft collected GPS data simultaneously. One aircraft, the Piper, flew altitude excursions from 0 to 1500 m. The other, an EC24, ranged from 0 to 5000 m. Positioning these two aircraft can provide an empirical answer to the question of whether the PAN solution errors depend upon altitude variations.

Since the aircraft experienced height variations, a necessary modification was made to the tropospheric model in the code that computes the simulated PPS solutions. The model uses surface weather values in its computation of the tropospheric delay. These surface values were modified to account for the changes in altitude of the aircraft.

Truth for the aircraft was obtained from On-The-Fly (OTF) kinematic solutions between the known reference site MSI and the aircraft. The kinematic solutions have demonstrated centimeter-level accuracies over short- to medium-length distances. Thus, these kinematic solutions should provide an accurate representation of the true aircraft position, given that the expected errors in the navigation solutions are an order of magnitude larger. The GDOP and the RMS solution residuals are plotted in Figures 21 and 22 for MSI on days 237 and 238, respectively. The PAN residuals (open circles) are computed from Equation (4). Since the ground track repeats from day-to-day with only a 4-min shift in time, the GDOP on the two days is approximately the same. The reason for the difference in the residual levels is unexplained. For day 237 at the static site MSI, the simulated PPS and PAN solutions were computed and are plotted in Figures 23 and 24, respectively. Results for day 238 are shown in Figures 25 and 26.
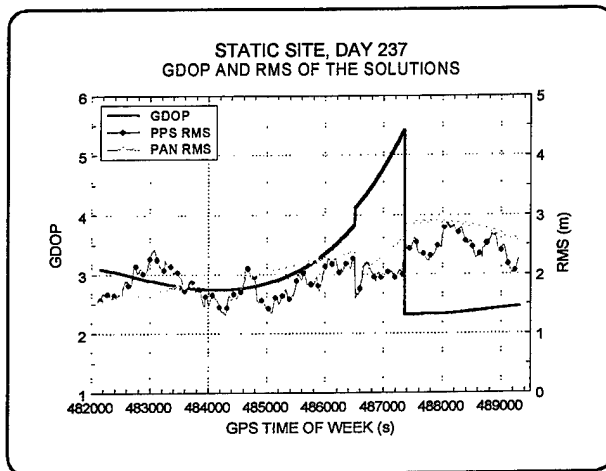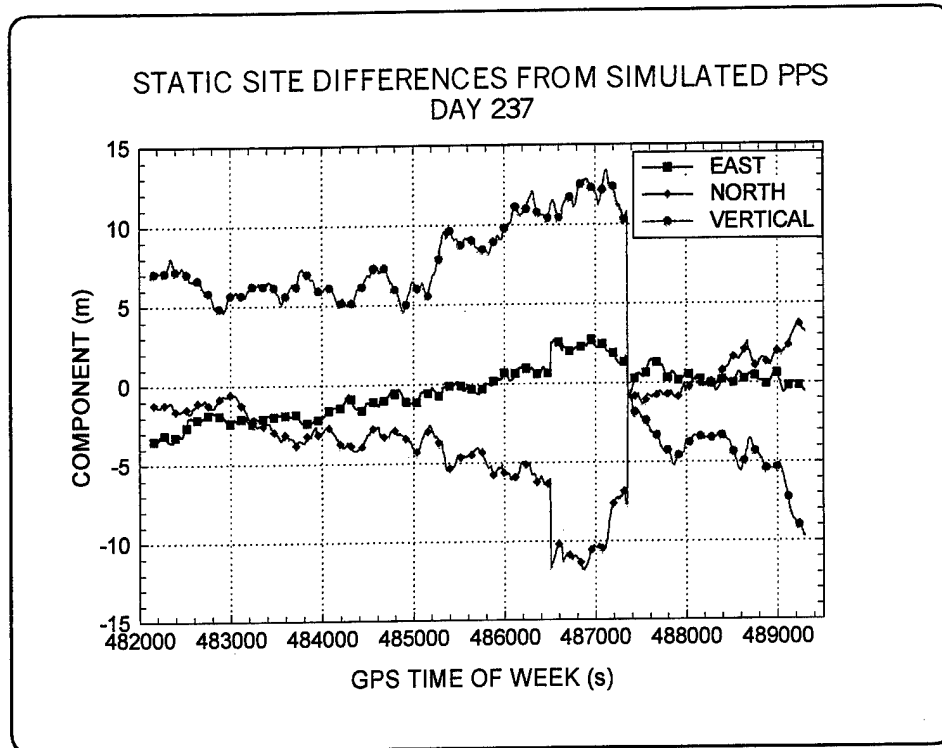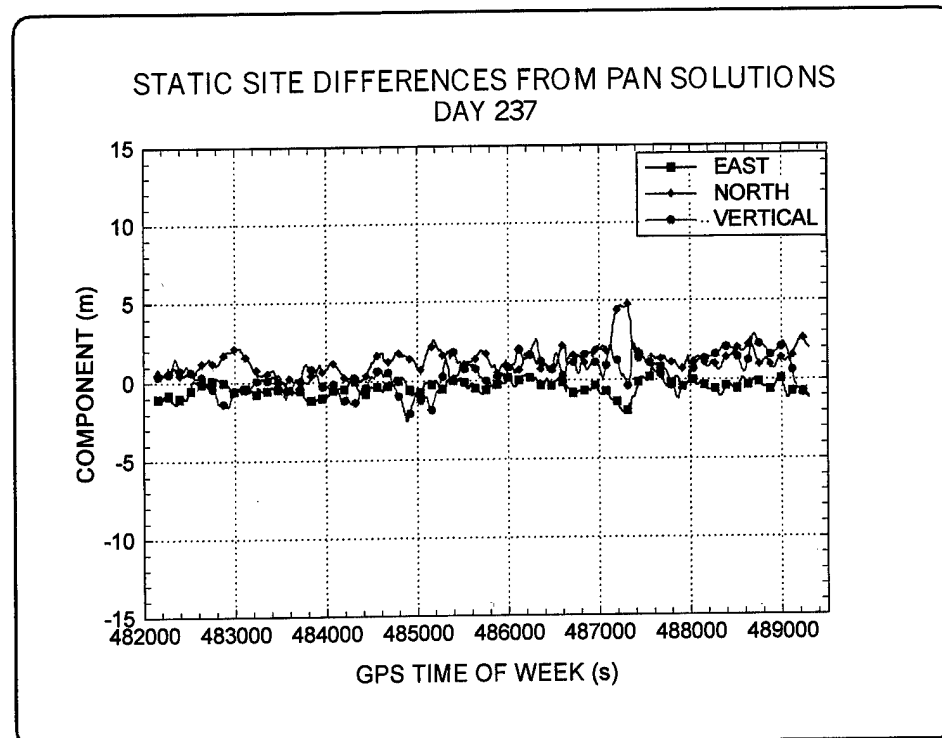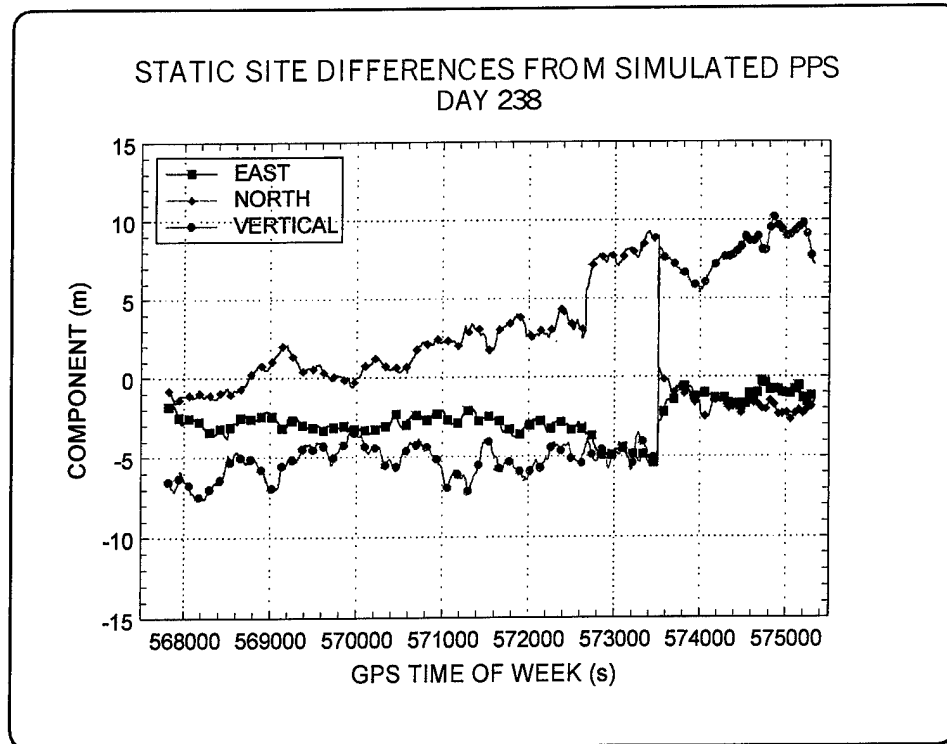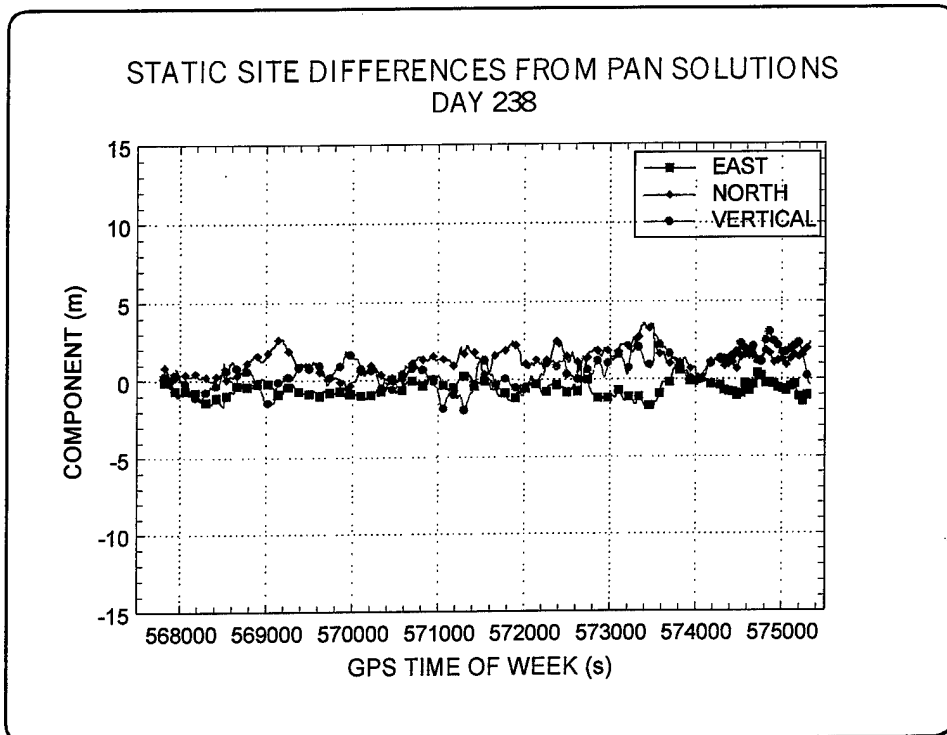

Figure 21—GDOP and RMS Residuals for MSI on Day 237
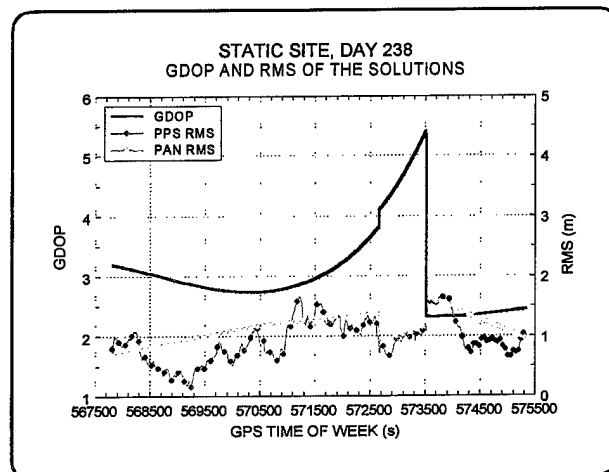
Figure 22—GDOP and RMS Residuals for MSI on Day 238

Figure 23—PPS Solutions at MSI on Day 237

Figure 24—PAN Solutions at MSI on Day 237
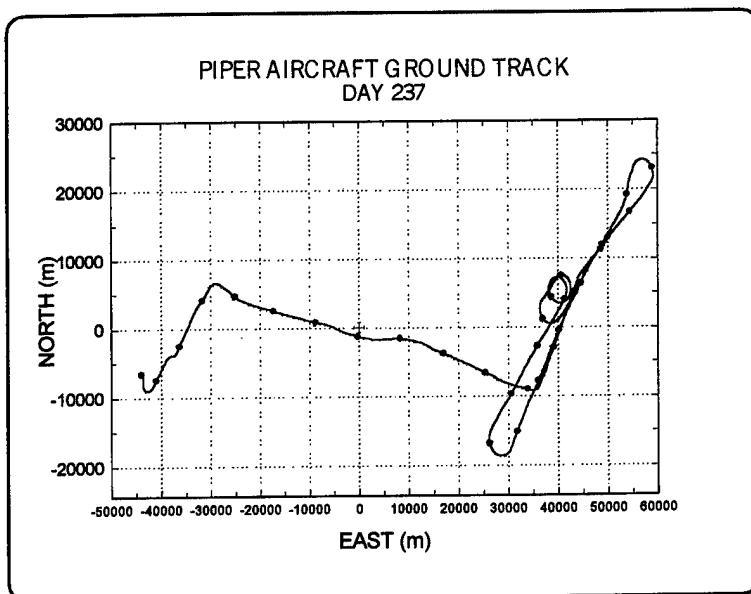
Figure 25—PPS Solutions at MSI on Day 238

Figure 26—PAN Solutions at MSI on Day 238

A summary of the results for MSI on both days is shown in Table 3. The nonzero means of these solutions indicate that there may be an offset in the given position for MSI. If this is the case, it can be subtracted from the aircraft solutions in order to give better agreement with the relative positions from the OTF truth.

Table 3—Summary of MSI Solutions

Units = meters	DAY 237			DAY 238		
	EAST	NORTH	VERTICAL	EAST	NORTH	VERTICAL
PPS						
Mean	-0.47	-3.09	4.54	-2.41	0.71	-0.17
Std. Dev.	1.49	3.43	5.95	1.20	2.96	6.67
PAN						
Mean	-0.48	1.16	0.39	-0.58	1.19	0.78
Std. Dev.	0.47	0.81	1.04	0.48	0.73	1.05

The East-West ground track for the Piper aircraft on day 237 is shown in Figure 27 for the period of time that truth was available. Symbols in the figure are plotted every minute, and the reference site, MSI, is at the origin. Each of the three component differences between the PPS solutions and the truth is plotted as a function of the GPS time of week in Figure 28. The ellipsoid height truth is also included in this figure as the open circles. The PAN results are shown in Figure 29. In this data set, the OTF kinematic truth solutions were established while the aircraft was still on the ground. The climb to altitude is indicated by the steep increase in ellipsoid height. There is no indication in the component differences (east, north, or vertical) that the error was greater during the time the aircraft was climbing than while on the ground, or at any other time while it was flying at a constant altitude. This is true for both PPS and PAN solutions. The two flights described next give evidence for a similar null result.

Figure 27—Ground Track for Piper Aircraft on Day 237

Figure 28—PPS Solutions for the Piper Aircraft on Day 237
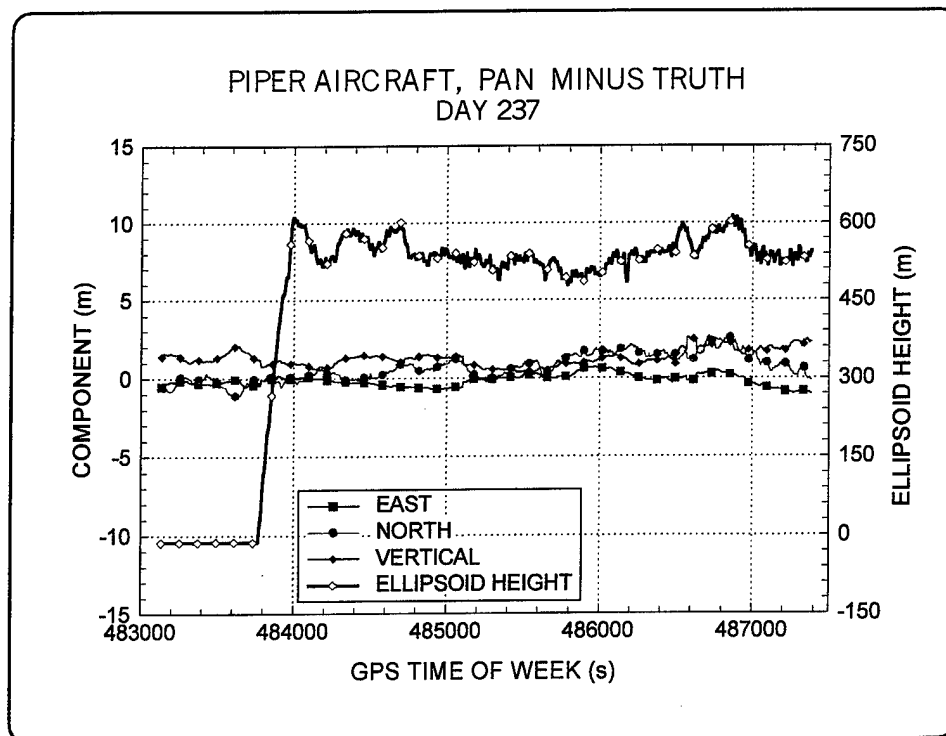
Figure 29—PAN Solutions for the Piper Aircraft on Day 237

The truth track for the Piper aircraft on day 238 is shown in Figure 30. The path is somewhat different than day 237, but the results are similar. The ellipsoid height and the three component differences are plotted in Figures 31 and 32. After the initial climb to about 500 m, the aircraft continued on up to 1500 m before descending again to 500 m. There is no evidence of extra position errors due to the changes in altitude. The results of the two Piper flights are summarized in Table 4.
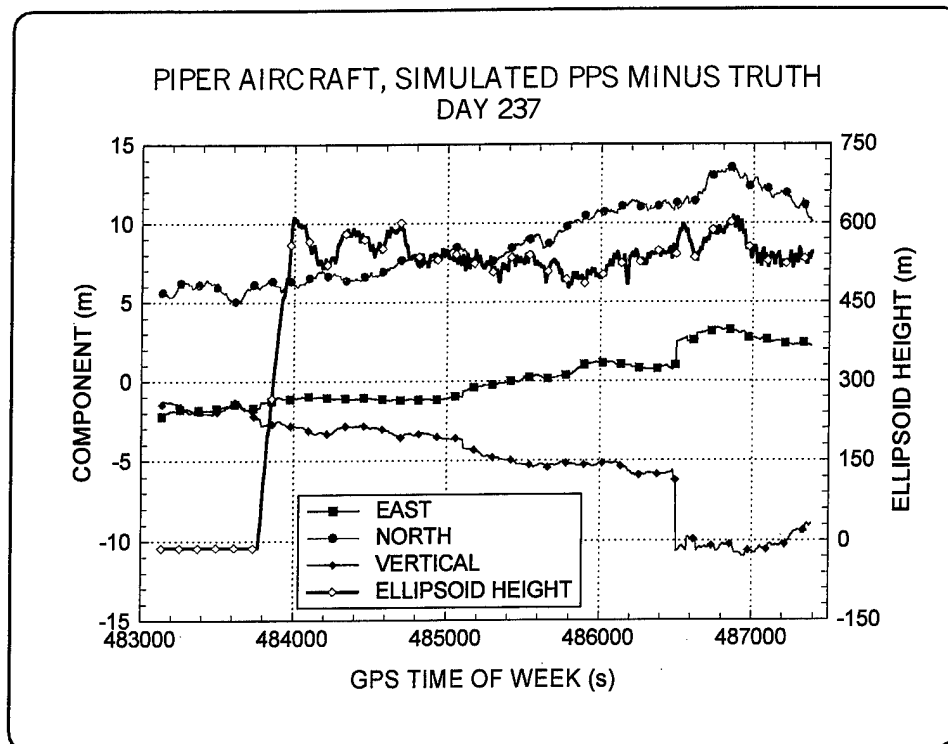

Figure 30—Piper Aircraft Ground Track for Day 238
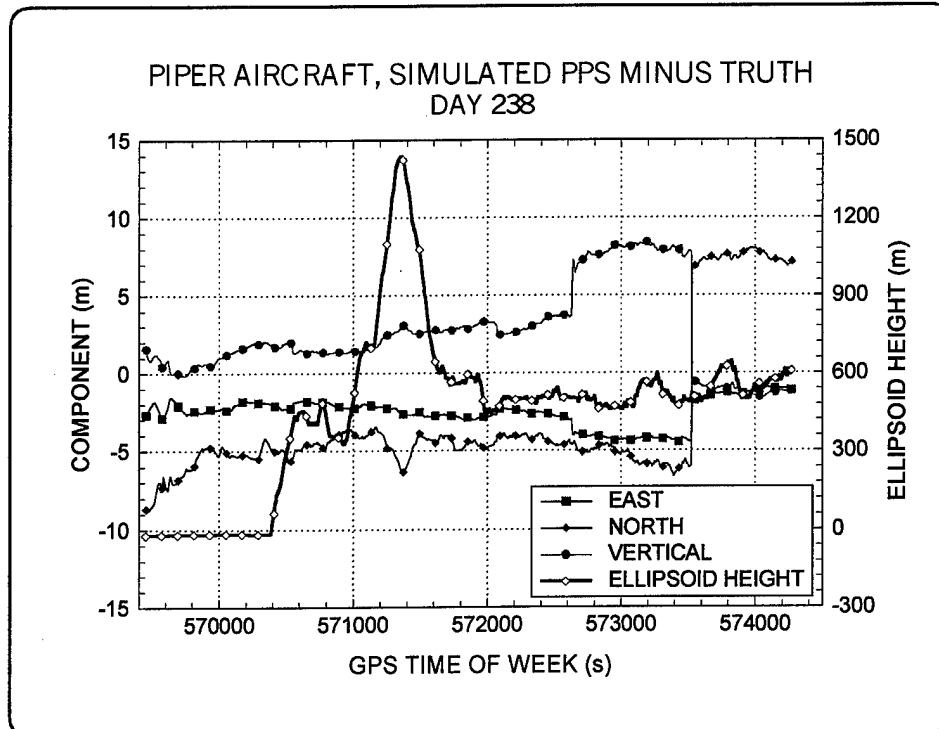
Figure 31—PPS Solutions for the Piper Aircraft on Day 238
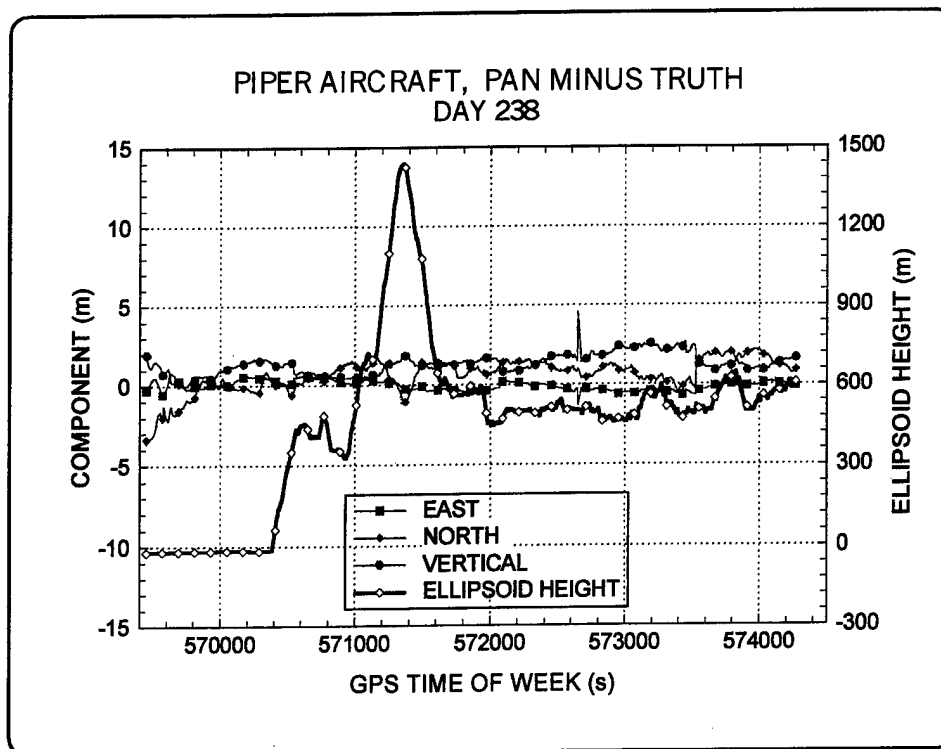
Figure 32—PAN Solutions for the Piper Aircraft on Day 238

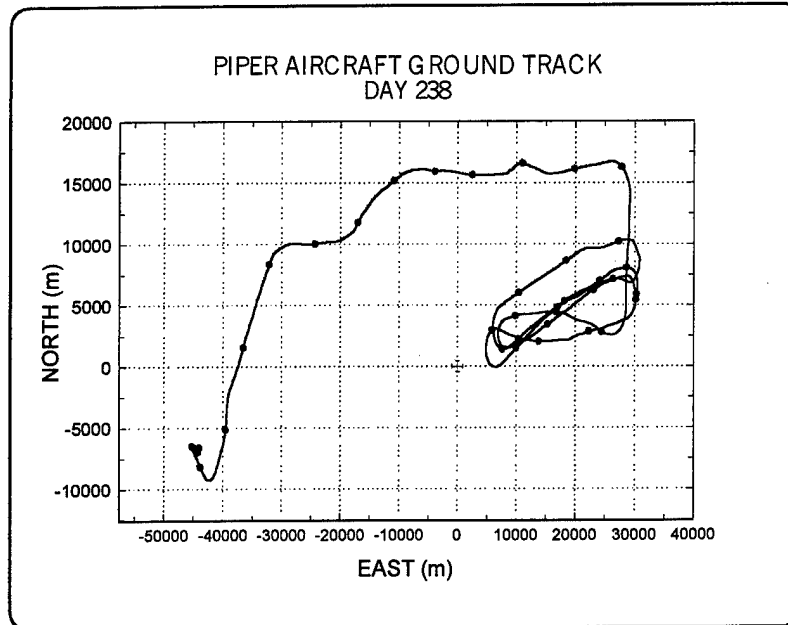The apparent mean component errors (PAN minus truth) can be reduced if the mean component offsets found at the MSI site, listed in Table 3, are subtracted from Table 4. The truth vector is measured from antenna to antenna. The aircraft truth position is computed as the *given* MSI position plus the truth vector. PAN results are positions of each antenna independently. If there is a position error at the MSI reference site, it can be subtracted from each aircraft position to form better agreement with the truth. When this is done, the mean difference between the PAN Piper solutions and the truth on day 237 is reduced to 0.30, 0.10, and 0.28 m in the east, north, and vertical directions, respectively. On day 238, these differences are 0.47, 0.08, and -0.23, respectively.

Table 4—Summary of Piper Aircraft Solutions

Units = meters	DAY 237			DAY 238		
	EAST	NORTH	VERTICAL	EAST	NORTH	VERTICAL
PPS						
Mean	0.09	-5.04	8.52	-2.54	2.57	-3.10
Std. Dev.	1.61	2.96	2.85	0.94	2.87	4.59
PAN						
Mean	-0.19	1.25	0.67	-0.11	1.27	0.55
Std. Dev.	0.37	0.50	0.81	0.34	0.58	0.98

The last test of PAN solution sensitivity to altitude variations was also carried out on day 238. The EC24 aircraft truth ground track is shown in Figure 33. It flew at a higher altitude and a greater distance from the MSI reference site. It also flew faster. This is evident by the larger distance between the 1-min symbols in Figure 33 compared with Figure 30. The ellipsoid height is plotted, along with the component differences in Figures 34 and 35 for PPS and PAN solutions, respectively. The results for all these cases show no increase in the solution error during periods of altitude changes. The summary of the single EC24 flight is shown in Table 5. If the mean values from MSI on day 238 are subtracted, the disagreement between the mean PAN solutions and the mean truth reduces to 0.35, -0.23, and -0.41 in the east, north, and vertical components respectively.

Figure 33—Ground Track of the EC24 Aircraft on Day 238

The conclusion that there is no evidence of position error as a function of altitude changes is what should be expected, since the GPS position accuracies are dependent primarily on the GDOP,
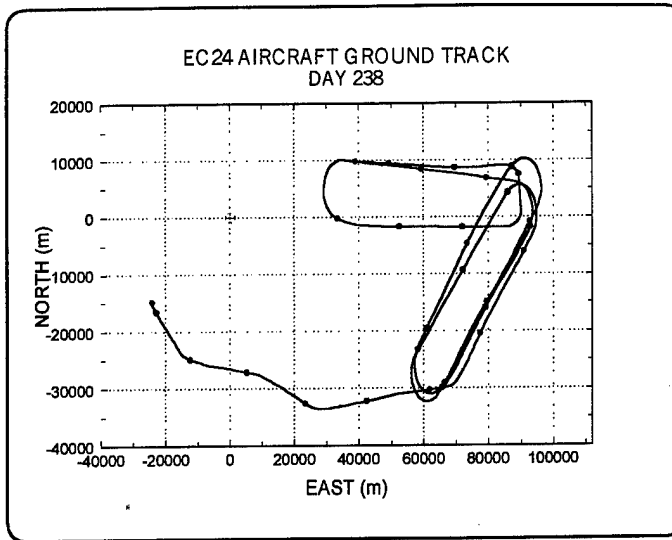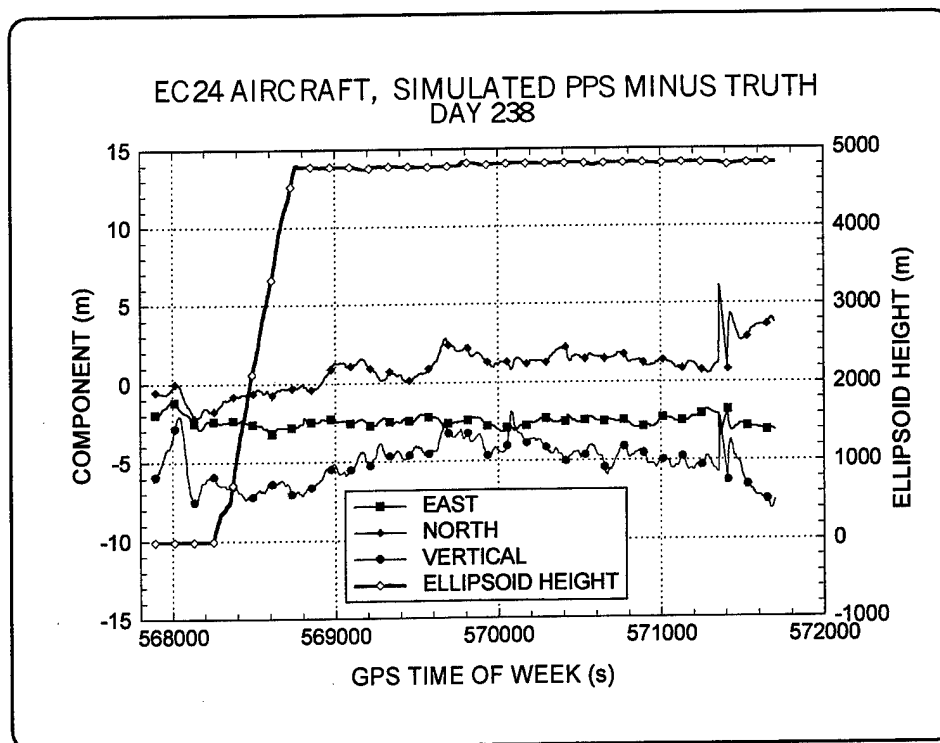

Figure 34—PPS Solutions for the EC24 Aircraft on Day 238
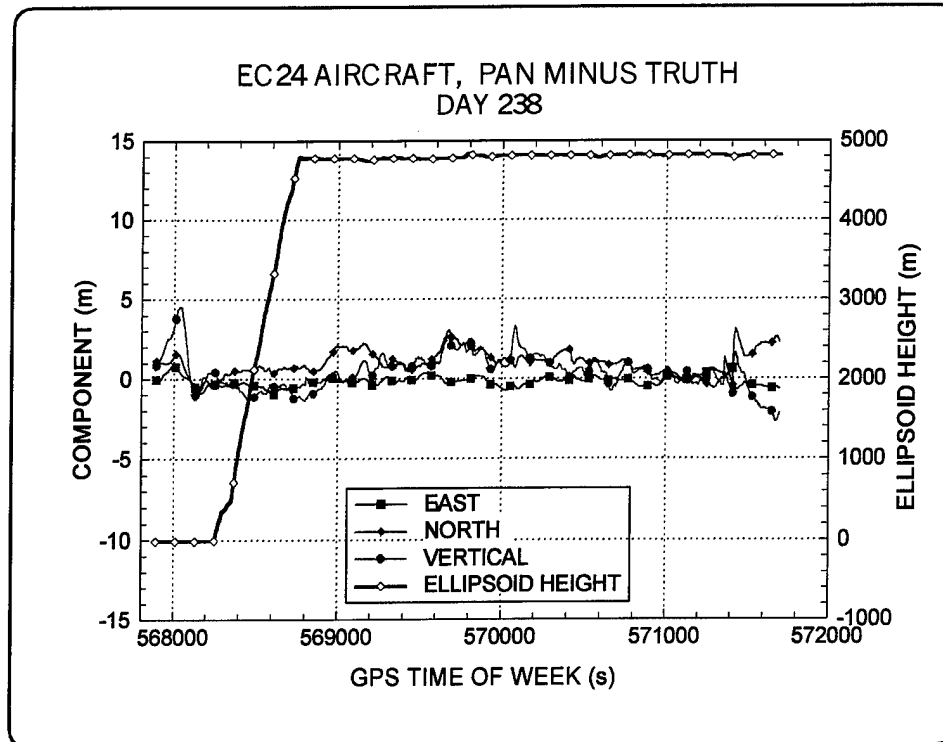
Figure 35—PAN Solutions for the EC24 Aircraft on Day 238

the ephemeris and clock errors, and the effects of multipath. Constant velocities due to the user should not introduce additional errors into the solutions. However, high accelerations may cause the receiver tracking loops to lag and may, in fact, introduce errors. For this effect to be apparent, the accelerations would need to be far greater than those encountered on these low-dynamic aircraft flights. Tracking loop errors due to vehicle accelerations may have been encountered on a rocket sled test at Holloman Air Force Base [9]. Additional position solutions, with observations collected by vehicles traveling along highways, are described in a previous report [10].

Table 5—Summary of the EC24 Aircraft Solutions on Day 238

Units = meters	DAY 237			DAY 238		
	EAST	NORTH	VERTICAL	EAST	NORTH	VERTICAL
PPS						
Mean				-2.50	0.87	-5.10
Std. Dev.				0.35	1.30	1.26
PAN						
Mean				-0.23	0.95	0.37
Std. Dev.				0.32	0.77	1.15

4.0 UAV SIMULATION

Missions for UAV include reconnaissance and remote targeting. When performing these missions, the position of the vehicle in flight at particular time epochs is required. The GPS has the potential to provide this information if a receiver is carried on board. If the real-time solutions are recorded and later recovered, the trajectory of the UAV can be upgraded with the precise ephemerides after mission completion. This is a good application for the PAN algorithm. The accuracy of postmission positioning with the precise ephemerides is investigated in this section.

4.1 The Method

Two computer programs were written to perform this simulation. The first produces the UAV flight path. Its output is a file containing the World Geodetic Coordinate System 1984 (WGS 84) coordinates as a function of time. The user inputs to this program include a WGS 84 starting point, a horizontal and vertical speed, and a direction. The vehicle position is computed at equally spaced time intervals until the time for the next maneuver is reached. The maneuvers may be a turn to a new azimuth, a change in speed, or a change in altitude. These maneuvers may be initiated at any time by editing the configuration file.

The second program reads the vehicle positions from the trajectory file and the satellite information from precise ephemerides. Pseudorange observations are computed by differencing the vehicle position from the satellites in view as determined from the ephemerides. Errors are introduced into the observations to simulate relativity, the ionospheric and tropospheric refraction, the local and satellite clock errors, and Gaussian random noise. SA errors are not included since it is assumed that a real UAV would produce SA-corrected solutions.

With the simulated pseudoranges written onto a RINEX-formatted file, the simulated PPS solutions are computed by the navigation solution algorithm using broadcast ephemerides in the usual way. These PPS solutions simulate those that would have been recorded by the UAV in flight. Finally, the solutions are upgraded with the precise ephemerides by the PAN algorithm. The results of this procedure are presented in the following section.

4.2 An Example Trajectory

A sample trajectory was generated beginning at a position near Kansas City. Initially the vehicle was flying south at about 55,000 ft. It then turned east to begin a series of overlapping tracks to simulate a reconnaissance of the area. The ground track is shown in Figure 36.

The position solutions from the simulated observations provide the PPS real-time results. These solutions and the precise ephemerides allow the PAN-improved results to be computed. The truth position is known from the simulated trajectory file. The differences between the simulated solutions

and this truth are illustrated in Figures 37 through 39. The satellite elevation cutoff angle for the solutions shown was taken as 10 deg. In this simulation, a lower elevation cutoff angle gives a smaller error. However, this improvement may not be realistic because aircraft banking and satellite dropouts due to obstruction by the airframe and the effects of multipath were not considered.
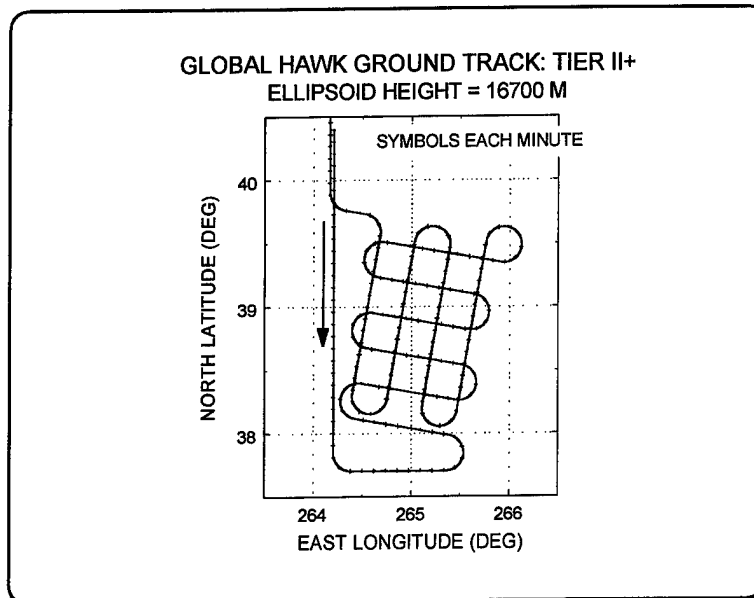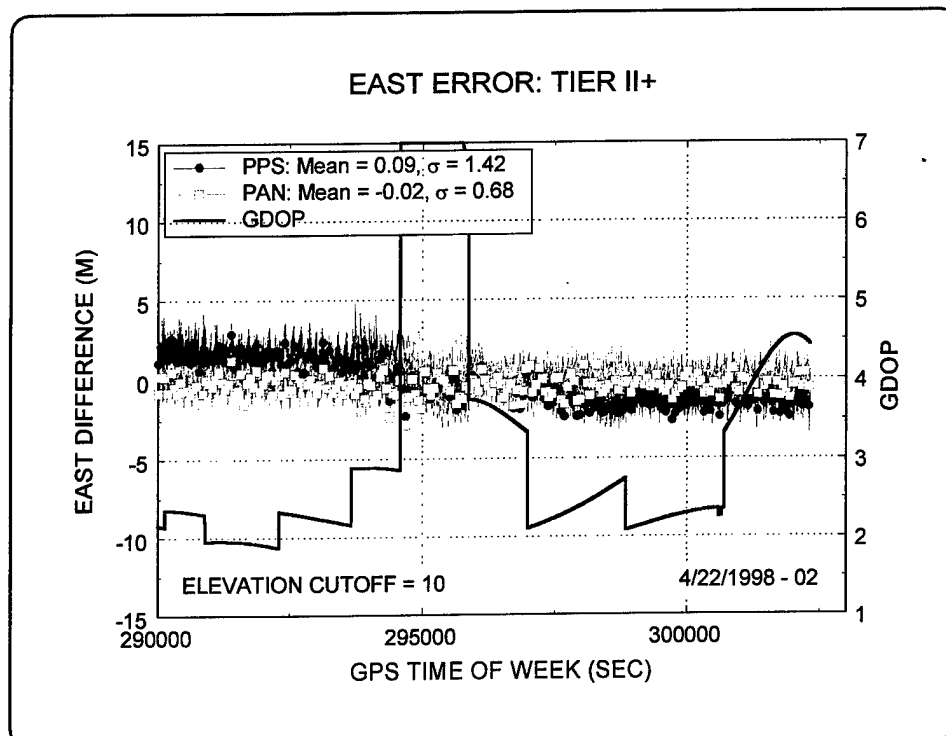

Figure 36—The UAV Ground Track

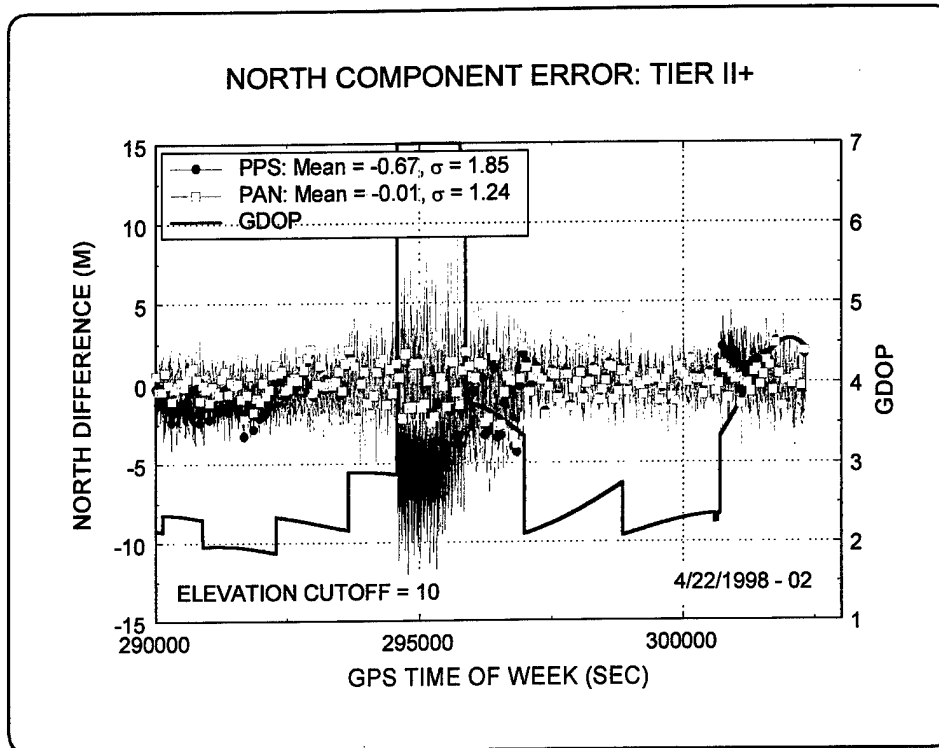**Figure 37**—The East Component Error
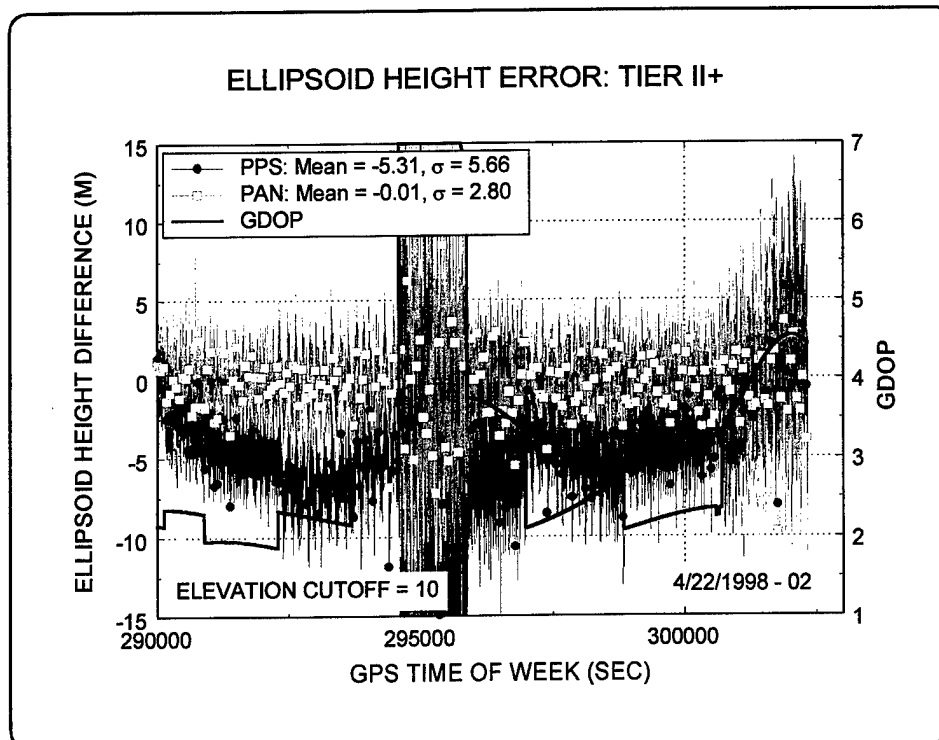
Figure 38—The North Component Error

Figure 39—The Ellipsoid Height Component Error

In the figures, the lines with the open symbols are the PPS solution errors; the lines with the filled symbols are the PAN solution errors. The solid line, the GDOP, indicates the geometric strength of the satellite constellation on the righthand axis. The means and standard deviations of the errors in the simulated solutions are listed in Table 6.

As expected, the mean errors from the PAN solutions are near zero. This is because the precise ephemerides were used both to generate the observations and to perform the PAN solutions. The PPS solutions used the broadcast ephemerides for the satellite positions. Therefore any differences between the broadcast ephemerides and the precise ephemerides are expressed in the differences between the PPS and the PAN solutions. A similar argument can be made to explain the larger standard deviations of the PPS solutions. Note that the figures illustrate that the error increases when the GDOP values are high. High GDOP implies a poor geometry due to the placement of the satellites in the sky or a lack of satellites. Both of these conditions may be expected to exist from time-to-time during aircraft flights due to blockages, as indicated previously. Therefore, the placement of the antenna on the aircraft is an important aspect of the overall positioning performance.

The trajectory generator and data generator developed for this simulation could be used to create observations for other flight paths and platforms. Both could be extended to include satellite dropouts due to antenna blockages if specifics about the aircraft attitude performance were known.

Table 6—Component Errors for the UAV Simulation

Units = meters	EAST		NORTH		UP	
	MEAN	S.D.	MEAN	S.D.	MEAN	S.D.
PPS	0.09	1.42	-0.67	1.85	-5.31	5.66
PAN	-0.02	0.68	-0.01	1.24	-0.01	2.80

5.0 SUMMARY AND CONCLUSIONS

The PAN formulation has been described, and examples of its performance have been presented. The first performance evaluation described was a comparison between solutions derived from single-frequency observations plus the broadcast ionospheric model and the two-frequency ionospherically corrected solutions. The solutions using the Klobuchar model, during a period of sunspot minimum, compared with the two-frequency results, gave good agreement.

The second evaluation was the performance of PAN during periods of rapidly varying altitude. Observations from two aircraft in flight were used to look for any increase in error during climbs. The results from this investigation were negative. There were no apparent differences in the quality of the solutions during changes in altitude when compared with straight and level flight.

The final performance evaluation required the generation of synthetic observations to simulate the data that might be collected by a high-altitude vehicle, such as a UAV. An example trajectory was

created, synthetic observations were generated, and simulated PPS solutions were obtained. These solutions were then used with the precise ephemerides to make PAN-improved solutions. The errors between the truth and the solutions were presented.

The results from all these tests showed that the PAN algorithm performs as expected and is not affected by low dynamic motion of the vehicle. High dynamics have not been tested, but there is no reason to expect it not to perform well in all types of environments.

6.0 REFERENCES

1. Hermann, Bruce R., "Five Years of Absolute Position at the Naval Surface Warfare Center," *Proceedings of the Sixth International Geodetic Symposium on Satellite Positioning*, The Ohio State University, March 1992.

2. Malys, Stephen; Bredthauer, Dennis; Hermann, Bruce; and Clynch, James, "Geodetic Point Positioning with GPS: A Comparative Evaluation of Methods and Results," *Proceedings of the Sixth International Geodetic Symposium on Satellite Positioning*, The Ohio State University, March 1992.

3. Lachapelle, G.; Klukas, R.; Roberts, D.; Qiu, W.; and McMillan, C., "One-Meter Level Kinematic Point Positioning Using Precise Orbits and Satellite Clock Corrections," *Proceedings of ION GPS-94*, Salt Lake City, Utah, September 1994.

4. Leach, Mark, private communication: 15 September 1995.

5. Hermann, Bruce R. and Risinger, Bonnie S., *Precise Absolute Navigation: An Evaluation of PPS Position Improvement*, NSWCDD/TR-95/196, October 1995.

6. Klobuchar, John A., "Ionospheric Time-Delay Algorithm for Single-Frequency GPS Users," *IEEE Transactions on Aerospace and Electronic Systems*, **AES-23**, No. 3, May 1987.

7. Parkinson, Bradford W.; Spilker, James J., Jr.; Axelrad, Penina; and Enge, Per, "Global Positioning System: Theory and Applications," Volume 1, *Progress in Astronautics and Aeronautics*, **163**, 1966, pg. 513.

8. Newby, Simon P. and Langley, Richard B., "Three Alternative Empirical Ionospheric Models – Are They Better Than the GPS Broadcast Model?," *Proceedings of the Sixth International Geodetic Symposium on Satellite Positioning*, The Ohio State University, Columbus, Ohio, March 1992.

9. Evans, Alan G.; Hermann, Bruce R.; Remondi, Benjamin W.; Simpson, Philip B.; Feist, Jon L.; and Wiles, George C., "An Evaluation of Precise Kinematic On-The-Fly Relative GPS Positioning for a Rocket Sled Test," *Proceedings of the 52nd Annual Meeting of the Institute of Navigation*, Cambridge, MA, June 19-21, 1996.

10. Hermann, Bruce R., *Performance Evaluation of Precise Absolute Navigation (PAN) Solutions over Four Test Courses*, Technical Report NSWCDD/TR-98/61, NSWCDD, Dahlgren, VA, January 1999.

DISTRIBUTION

	Copies		Copies
DOD ACTIVITIES (CONUS)		**INTERNAL**	
ATTN S MALYS	5	B60	3
NIMA/ TRB		K43 SITZMAN	1
MAIL STOP P53		K43 MELKUN	1
12300 SUNRISE VALLEY DR		T10	1
RESTON VA 20191-3448		T12	2
		T12 SWIFT	1
ATTN R SMITH	5	T12 CUNNINGHAM	1
NIMA/ TR		T12 DURLING	1
MAIL STOP P-53		T12 EVANS	1
12300 SUNRISE VALLEY DR		T12 FUTCHER	1
RESTON VA 20191-3448		T12 HERMANN	10
		T12 O'TOOLE	1
ATTN ANGUS JONES	5	T13	1
NIMA/GIMGD MS L-41			
3200 S SECOND ST			
ST. LOUIS MO 63118			

COMMANDING OFFICER
CSSDD NSWC
6703 W HIGHWAY 98
PANAMA CITY FL 32407-7001   1

DEFENSE TECH INFORMATION CTR
8725 JOHN J KINGMAN RD
SUITE 0944
FORT BELVOIR VA 22060-6218   2

NON-DOD ACTIVITIES (CONUS)

THE CNA CORPORATION
PO BOX 16268
ALEXANDRIA VA 22302-0268   1

ATTN MICHAEL ALBIN CHIEF   1
ANGLO/AMERICAN ACQUISITIONS
        DIVISION
LIBRARY OF CONGRESS
101 INDEPENDENCE AVENUE SE
WASHINGTON DC 20540-4170